CASE FILE
COPY

NACA TN 4191

NATIONAL ADVISORY COMMITTEE FOR AERONAUTICS

TECHNICAL NOTE 4191

ANALYSIS OF HORIZONTAL-TAIL LOADS IN PITCHING MANEUVERS ON A FLEXIBLE SWEPT-WING JET BOMBER

By William S. Aiken, Jr.

Langley Aeronautical Laboratory
Langley Field, Va.

Washington
December 1957

X

NATIONAL ADVISORY COMMITTEE FOR AERONAUTICS

TECHNICAL NOTE 4191

ANALYSIS OF HORIZONTAL-TAIL LOADS IN PITCHING MANEUVERS ON A FLEXIBLE SWEPT-WING JET BOMBER

By William S. Aiken, Jr.

SUMMARY

Horizontal-tail loads measured by means of strain gages in pitching maneuvers are analyzed to determine wing-fuselage aerodynamic-center position, zero-lift pitching-moment coefficient, airplane pitching moment of inertia, and radius of gyration. A similar analysis is made of the time-history data for the elevator angles and the results were found to agree with those from the tail-load analysis. The flight-determined values of aerodynamic-center position for rigid conditions and the zero-lift pitching-moment coefficients were in some disagreement with the wind-tunnel data over the Mach number range of the tests (0.42 to 0.81). The pitching moment of inertia determined from the flight data for rigid-wing conditions agreed with calculations based on ground tests. The effective pitching moment of inertia computed from theoretical consideration for flexible flight conditions was in disagreement with flight data. Details of the analysis procedures and least-squares methods used are given.

INTRODUCTION

The calculation of airplane design tail loads and stability characteristics requires reliable estimates of the wing-fuselage pitching-moment characteristics. The use of highly swept flexible wings combined with other flexible airplane components introduces additional factors which must be considered in tail-load design analysis procedures. Investigations by the National Advisory Committee for Aeronautics of a large flexible swept-wing jet bomber which included measurements of horizontal-tail loads permitted the analysis of data from which comparisons could be made between wind-tunnel measurements of wing-fuselage aerodynamic-center positions and zero-lift pitching-moment coefficients and values of these parameters as derived from flight data.

The analysis of flight data in the present report is, to a large extent, based on analyses and information contained in references 1

and 2 for wing deflections, reference 3 for horizontal-tail parameters, reference 4 for airplane lift-curve slopes and angles of zero lift, and reference 5 for wing centers of pressure. The methods used to analyze the flight data and to convert measured pitching-moment parameters to equivalent rigid conditions for comparison with wind-tunnel data are described in detail. Comparisons are given between flight and wind-tunnel results for aerodynamic-center position and zero-lift pitching-moment coefficients and between flight and calculated values of moments of inertia and radii of gyration for both flexible and rigid conditions. Although no direct comparisons are made with present tail-load design computation methods, the theoretical methods which were used in the flight-data analysis contain the essential elements of design procedures for flexible aircraft and, thus, provide an indirect check on their adequacy.

SYMBOLS

A,B,C,D coefficients of equations (A7) and (B1) used to obtain airplane pitching-moment parameters

A_{corr} the A coefficient of equation (B1) corrected for zero shift

$C_{L_{\alpha_t}}$ horizontal-tail lift-curve slope per degree

$\left(C_{L_{\alpha_t}}\right)_f$ horizontal-tail lift-curve slope per degree for flexible fuselage conditions defined by the expression

$$\frac{C_{L_{\alpha_t}}}{1 - \frac{di_t}{dL_t} C_{L_{\alpha_t}} qS_t}$$

C_{L_δ} horizontal-tail lift-curve slope per degree with root elevator angle

C_{m_δ} tail pitching-moment coefficient due to elevator deflection

C_{m_0} zero-lift wing-fuselage pitching-moment coefficient

$C_{m_{0_M}}$ zero-lift wing-fuselage pitching-moment coefficient computed directly from measured zero-lift tail load

$C_{M_{0_I}}$ corrected zero-lift wing-fuselage pitching-moment coefficient using analysis method I

$C_{m_{O_{II}}}$ zero-lift wing-fuselage pitching-moment coefficient using analysis method II

$C_{N_{A_C}}$ airplane normal-force coefficient corrected for pitching-acceleration tail load

I_y airplane pitching moment of inertia, slug-ft^2

I_{y_f} effective airplane pitching moment of inertia defined by equation (A10), slug-ft^2

L_t aerodynamic tail load, lb

L_{t_T} aerodynamic tail load plus component of tail aerodynamic pitching moment defined by equation (A6), lb

L_w aerodynamic wing load, lb

$L_{w_{\ddot{\theta}}}$ aerodynamic wing load per unit pitching acceleration, $\frac{\text{lb}}{\text{radian/sec}^2}$

$L_{\dot{\theta}}$ aerodynamic wing load due to pitching velocity (eq. (A3)), lb

$L_{\ddot{\theta}}$ aerodynamic wing load due to pitching acceleration (eq. (A2)), lb

M Mach number

M_{ac} pitching moment about wing-fuselage aerodynamic center

N number of equations in least-squares solutions

S wing area, sq ft

S_t horizontal-tail area, sq ft

T_t tail aerodynamic torque, in-lb

V true airspeed

W airplane weight, lb

W_t horizontal-tail weight, lb

X_{cg} location of airplane center of gravity, percent $\bar{c}$

$(X_{ac})_r$ location of rigid-wing—fuselage additional-load aerodynamic center, percent $\bar{c}$

$(X_{ac})_{flex}$ location of flexible-wing—fuselage additional-load aerodynamic center, percent $\bar{c}$

$X_{\ddot{\theta}}$ location of center of pressure of aerodynamic wing load due to pitching acceleration, percent $\bar{c}$

Z' zero shift in measured aerodynamic tail loads (from ref. 3), lb

Z_T zero shift in measured aerodynamic tail torque, in-lb

a_F faired tail-on airplane lift-curve slope per degree (from ref. 4)

$\bar{c}$ wing mean aerodynamic chord, in.

$\bar{c}_t$ tail mean aerodynamic chord, in.

d distance from wing-fuselage aerodynamic center to airplane center of gravity, positive with center of gravity forward of the aerodynamic center, in.

$d_{\ddot{\theta}}$ center of pressure of wing load due to pitching acceleration, in.

$d_{\dot{\theta}}$ center of pressure of wing load due to pitching velocity, in.

g acceleration of gravity, ft/sec^2

i_t tail incidence, deg

i_w wing incidence, deg

k_y airplane radius of gyration in pitch, ft

k_{y_f} effective airplane radius of gyration in pitch, ft

l_t horizontal-tail length, distance from airplane center of gravity to quarter-chord of horizontal-tail mean aerodynamic chord, in.

m_R rigid-wing—fuselage lift-curve slope per degree

n normal load factor at airplane center of gravity

n_t normal load factor at horizontal tail

q dynamic pressure, lb/sq ft

w weighting factors

x_t distance from wing-fuselage aerodynamic center to quarter-chord of horizontal-tail mean aerodynamic chord, in.

ΔX_{ac} difference between rigid- and flexible-wing—fuselage aerodynamic-center positions, defined by equation (6), percent $\bar{c}$

$\Delta k_{y_f}{}^2$ difference between theoretical and measured $k_{y_f}{}^2$ values, ft^2

α_t tail angle of attack, deg

α_w wing angle of attack, deg

$\alpha_{0_{adj}}$ wing angle of zero lift (from ref. 4), deg

δ root elevator angle, positive down, deg

δ_0 root elevator angle at zero load factor, deg

ϵ errors in fit or measurements; subscripts to ϵ denote error associated with quantity indicated

ϵ_1 error in calculated $k_{y_f}{}^2$

ϵ_2 error in measured $k_{y_f}{}^2$

$\dot{\theta}$ pitching velocity, radian/sec

$\ddot{\theta}$ measured pitching acceleration corrected for instrument response characteristics, radian/sec^2

$\sum$ indicates summation

$d\epsilon/d\alpha$ effective downwash factor

Matrix notation:

$\{\ \}$ column matrix

$\|\ \|$ rectangular matrix

$\|\ \|^T$ transpose of rectangular matrix

$[\ ]^{-1}$ inverse of square matrix

Bars over symbols indicate average values.

APPARATUS AND TESTS

Airplane

The airplane used for this investigation was a six-engine, jet-propelled medium bomber. A photograph of the test airplane is shown as figure 1, and the airplane and horizontal-tail characteristics and dimensions are given in table I.

Instrumentation

The data used for analysis in the present paper were obtained from standard NACA recording instruments and from strain gages mounted on the right and left sides of the horizontal tail.

Normal accelerations were measured by two air-damped accelerometers, one near the center of gravity and one at the horizontal tail. Angular accelerations in pitch were measured by a rate-gyro type, electrically differentiating, magnetically damped turnmeter. Airspeed and altitude measurements were made with an NACA pitot-static head mounted on a boom approximately 1 maximum fuselage diameter ahead of the original nose.

Electrical wire-resistance strain gages (Type A-6) with low temperature correction factors were used to measure the root shears, bending moments, and torques at stations on the right and left sides of the tail. The gages were installed as four-active-arm bridges on the web and flanges of the main spars (50 percent chord) and on the upper and lower skin surfaces near the leading edges of the horizontal tail.

The strain-gage bridge installation was calibrated according to the method detailed in reference 6. The bridges were then combined electrically so that, except for secondary carryover effects, a combined shear, moment, or torque bridge responded primarily to the shear, moment, or torque for the side of the tail on which the load was being measured. Final calibration equations using combined bridge outputs included carryover-effect corrections.

The combined strain-gage outputs were recorded on an 18-channel oscillograph with individual galvanometer responses flat to 60 cps. All data were evaluated by using nondimensional deflections as

$$\rho = \frac{\text{Flight deflection - Ground zero deflection}}{\text{Calibrate signal deflection}}$$

The sensitivity of each combined bridge was generally recorded prior to entering a maneuver through the use of a calibrate signal. With this system of data reduction, changes in battery voltage had no effect on the measurement of loads. In addition, galvanometer zeros with strain-gage power off were recorded to compensate for any mechanical shifts in the galvanometer zero position due to temperature effects in the recorder and any thermal electromotive-force effects in the strain-gage circuits.

Aerodynamic tail loads on the horizontal tail were obtained from the structural loads (measured by the strain-gage bridges) and the known tail weight and normal load factor from the equation

$$L_{t_{aero}} = L_{t_{struct}} - n_t W_t$$

The aerodynamic bending moments and torques were obtained in a similar manner.

The recorded data for all instruments were synchronized at 0.1-second intervals by means of a common timing circuit. All instruments were damped to about 0.67 of critical damping. A summary of pertinent quantities measured, instrument locations, and accuracies are given in the following table:

Quantity	Location	Instrument range	Instrument accuracy
Normal acceleration, g units	34.2 percent $\bar{c}$	0 to 2	0.005
Normal acceleration, g units	47.8 percent horizontal-tail root chord	-2 to 6	0.02
Pitching acceleration, radians/sec^2 . . .	25 percent $\bar{c}$	±0.50	0.01
Dynamic pressure, lb/sq ft	140 in. ahead of original nose	0 to 800	1
Static pressure, lb/sq ft	132 in. ahead of original nose	0 to 2,200	2
Tail shear, per side, lb	Root of tail	±25,000	60
Tail torque, per side, in-lb	Root of tail	±2,000,000	4,000

Tests

All tests were made with the airplane in the clean condition. The flight data evaluated in this report were taken from 68 push-down—pull-up maneuvers (the same maneuvers used in refs. 3 and 4) made at altitudes of 20,000, 25,000, 30,000, and 35,000 feet and an overall Mach number range from 0.427 to 0.812. The tests were made at normal and forward center-of-gravity positions and airplane weights ranging from 104,000 to 127,000 pounds. Table II is a summary of the flight conditions for these runs. In the table are listed the flight and run numbers, average Mach number, average dynamic pressure, test altitude, weight, and center-of-gravity position. The range of Mach number and dynamic-pressure changes during any test are also indicated. It might be noted that the center-of-gravity listings in table II differ slightly from those given for the same maneuvers in references 3 and 4. The airplane centers of gravity have been corrected for the effect of airplane attitude on the fuel-tank centers of gravity for the three large unbaffled fuselage tanks.

METHODS AND RESULTS

The airplane pitching-moment parameters, that is, wing-fuselage aerodynamic-center position and zero-lift pitching-moment coefficient, and the airplane effective moment of inertia may be evaluated from flight measurements of the airplane motions and the horizontal-tail load. In appendix A, use is made of the airplane pitching-moment equation to set up two methods of analysis amenable to least-squares treatment. The methods are:

Method I. A procedure in which direct tail-load measurements are used.

Method II. A procedure in which elevator-angle measurements are used.

Pitching-moment parameters obtained by the use of either method include quasi-static wing-flexibility effects but the equations do not allow for dynamic wing, tail, or fuselage frequency-response effects since the bulk of the data presented was obtained without excitation of the major airplane components.

The following sections present the determination of the pitching-moment parameters from flight time-history data and comparisons with available wind-tunnel and mass-distribution data. The method used for extrapolating or correcting the measured aerodynamic-center positions to rigid-wing conditions is given in detail. The theoretical relationship existing between the measured or effective moment of inertia and the actual or rigid-airplane moment of inertia is also described.

Basic Data

The least-squares data-reduction procedures as used for methods I and II are given in appendix B. These procedures are used for the evaluation of the required tail-load and elevator-angle coefficients for each of the 68 maneuvers studied. These tail-load and elevator-angle coefficients in turn are used for the evaluation of the airplane pitching-moment parameters. Both methods are illustrated by use of the time-history data for n, $\ddot{\theta}$, $\dot{\theta}l_t/V$, L_{t_T}, and δ shown in figures 2, 3, and 4 for an example maneuver (flight 12, run 27). The calculated tail-load and elevator-angle time histories from equations (B4) and (B6) are illustrated in figures 3 and 4, respectively.

It is demonstrated in appendix B that for method I a simplified form of equation (B2) which omits the $\dot{\theta}l_t/V$ term could be used for the

determination of the zero-lift tail load, the tail load per g, and the tail load per unit pitching acceleration. The A, B, and C coefficients of equation (B2), along with their standard errors and errors of fit, for each of the 68 maneuvers analyzed are given in table III.

The coefficients from the least-squares analysis of the elevator-angle data (method II), along with their standard errors and errors of fit, for each of the 68 maneuvers analyzed are given in table IV.

Aerodynamic-Center Position

The B coefficients of method I and the $\partial\delta/\partial n$ coefficients of method II, given in tables III and IV, respectively, as deduced from flight time-history data now permit the determination of the wing-fuselage aerodynamic-center location. This section illustrates the methods used to extract the aerodynamic-center data and to extrapolate the data as measured for flexible-wing conditions to rigid-wing conditions. In appendix A, equations (A8) and (A25) show the relationship between the aerodynamic-center position d (the distance between airplane center of gravity and wing-fuselage aerodynamic-center location) and the measured coefficients. A general equation expressing the aerodynamic-center position in terms of its location on the wing mean aerodynamic chord is

$$\left(X_{ac}\right)_{flex} = X_{cg} + \frac{d}{\bar{c}}\,100 \tag{1}$$

and is used to correlate the data obtained at various center-of-gravity locations.

Aerodynamic-center position using method I.- Equation (A8) of appendix A gives the aerodynamic-center location d as

$$d = \frac{Bl_t}{W - B} \tag{2}$$

Inserting numerical values for the example maneuver of appendix B with $B = 392$ (from eq. (B4)), $l_t = -552$ inches, and $W = 110{,}300$ pounds in equation (2) gives

$$d = -1.97 \text{ inches}$$

The aerodynamic center in terms of the mean aerodynamic chord, using equation (1) and the center-of-gravity position of 22.9 percent, thus becomes

$$\left(X_{ac}\right)_{flex} = 22.9 + \left(\frac{-1.97}{1.559}\right) = 21.6 \text{ percent}$$

The error in $\left(X_{ac}\right)_{flex}$ may be determined by use of the standard error in the B coefficient as

$$\epsilon_{X_{ac}} \approx \frac{\epsilon_B l_t}{W - B} \frac{100}{\bar{c}} \tag{3}$$

Using the standard error of B from table III gives

$$\epsilon_{X_{ac}} = \pm \frac{358(-552)}{(109,910)(1.559)} = \pm 1.2 \text{ percent}$$

The aerodynamic-center positions and the associated standard errors for each of the 68 maneuvers are given in table V.

Aerodynamic-center position using method II.- Equation (A25) of appendix A gives the aerodynamic-center location d as

$$d = \frac{l_t\left(C_{L_{\alpha_t}}\right)_f\left[\frac{\partial\delta}{\partial n}\frac{d\alpha_t}{d\delta} + \frac{di_t}{dn_t} + g\frac{l_t}{V^2}\frac{d\epsilon}{d\alpha} + \left(1 - \frac{d\epsilon}{d\alpha}\right)\frac{W}{a_F qS}\right] + \frac{\partial\delta}{\partial n}C_{m_\delta}\bar{c}_t}{\frac{W}{qS_t} - \left(C_{L_{\alpha_t}}\right)_f\left[\frac{\partial\delta}{\partial n}\frac{d\alpha_t}{d\delta} + \frac{di_t}{dn_t} + g\frac{l_t}{V^2}\frac{d\epsilon}{d\alpha} + \left(1 - \frac{d\epsilon}{d\alpha}\right)\frac{W}{a_F qS}\right]} \tag{4}$$

For use in equation (4) values of the parameters $\left(C_{L_{\alpha_t}}\right)_f$, $\frac{d\alpha_t}{d\delta}$, $\frac{d\epsilon}{d\alpha}$, and C_{m_δ} were obtained from reference 3 and the airplane lift-curve slope a_F was obtained from reference 4. The parameter $\frac{di_t}{dn_t}$ (tail-incidence change due to fuselage bending under inertia loads) was obtained from equation (7) of reference 3. The remaining parameters required are g, the acceleration of gravity, V, the true airspeed, and q, the dynamic pressure. The quantity $\partial\delta/\partial n$ is the coefficient of equation (A19) associated with n and is given in table IV.

For the example maneuver, substitution of numerical values into equation (4) results in

$$d = -3.22 \text{ inches}$$

The aerodynamic center by method II for the example maneuver is from equation (1):

$$\left(X_{ac}\right)_{flex} = 22.9 + \left(\frac{-3.22}{1.559}\right) = 20.8 \text{ percent}$$

The error in $\left(X_{ac}\right)_{flex}$ may be computed from the standard error of the $\frac{\partial\delta}{\partial n}$ coefficient given in table IV as

$$\epsilon_{X_{ac}} = \frac{\left[l_t\left(C_{L_{\alpha_t}}\right)_f \frac{d\alpha_t}{d\delta} + C_{m_\delta}\bar{c}_t\right]\epsilon_{\partial\delta/\partial n}\frac{100}{\bar{c}}}{\frac{W}{qS_t} - \left(C_{L_{\alpha_t}}\right)_f\left[\frac{\partial\delta}{\partial n}\frac{d\alpha_t}{d\delta} + \frac{di_t}{dn_t} + g\frac{l_t}{V^2}\frac{d\epsilon}{d\alpha} + \left(1 - \frac{d\epsilon}{d\alpha}\right)\frac{W}{a_F qS}\right]} \tag{5}$$

Using the standard error of $\partial\delta/\partial n$ from table IV gives

$$\epsilon_{X_{ac}} = \frac{\left[(-552)(0.0559)(0.420) + (-0.0086)103\right](\pm 0.258)}{1.559(2.562)} = \pm 0.9 \text{ percent}$$

The aerodynamic-center positions and their associated standard errors for all 68 maneuvers are given in table V where they may be compared with the values determined by using method I.

Extrapolation to rigid-wing conditions.- The aerodynamic-center-position data in table V are for flexible-wing conditions. If the effects of wing flexibility are known, the flight measurements may be extrapolated to rigid-wing conditions and the variation of aerodynamic-center position with Mach number established. Data are available in reference 5 which may be used for this extrapolation. The forward shift of the wing aerodynamic-center position as a function of the flexibility parameter qm_R is shown in figure 5, as determined from the theoretical curve (for an average value of $W = 110,000$ pounds) of figure 4(c) in reference 5 by conversion of the root center-of-pressure variation with qm_R to percent mean aerodynamic chord. Since the wing additional-load center-of-pressure data in figure 4(c) of reference 5 were determined from wing-root aerodynamic torques and the airplane center-line shear $\left(\frac{1}{2}nW - \frac{1}{2}L_t\right)$, the rigid-wing—fuselage aerodynamic-center position may be determined from the equation

$$\left(X_{ac}\right)_r = \left(X_{ac}\right)_{flex} + \Delta X_{ac} \tag{6}$$

When equation (6) is used it is assumed that the wing-fuselage aerodynamic-center position differs from the wing aerodynamic-center position only by a constant for any given Mach number and that changes in dynamic pressure do not affect the fuselage contribution to the total wing-fuselage aerodynamic-center position.

The values of qm_R for use in the determination of ΔX_{ac} from figure 5 are listed in table V and were obtained from the dynamic pressures given in table II and the rigid-wing—fuselage lift-curve slopes m_R given in reference 4. The $\left(X_{ac}\right)_r$ values obtained from equation (6) for the method I and method II data and the ΔX_{ac} values from figure 5 are given in table V. The values of $\left(X_{ac}\right)_r$ for both methods are plotted in figure 6 and are identified by method.

It will be noted that the errors associated with the aerodynamic centers $\epsilon_{X_{ac}}$ of table V are not constant. Use was made of these errors to define weighting factors to obtain weighted average values of aerodynamic center at the group Mach numbers indicated in table V. The weighting factor is defined as

$$w = \left(\frac{1}{\epsilon_{X_{ac}}}\right)^2 \tag{7}$$

and the weighted average aerodynamic-center position is defined by the equation

$$\left(\bar{X}_{ac}\right)_r = \frac{\sum w\left(X_{ac}\right)_r}{\sum w} \tag{8}$$

The standard error of the weighted average is given by the equation

$$\epsilon_{\bar{X}_{ac}} = \sqrt{\frac{\sum w\left(X_{ac}\right)_r^2 - \left(\bar{X}_{ac}\right)_r \sum w\left(X_{ac}\right)_r}{N \sum w}} \tag{9}$$

The last column of table V gives the weighted average values of the aerodynamic-center position and the standard errors computed using equations (8) and (9) for the Mach number groups used. These weighted average

aerodynamic-center values are also plotted as circles in figure 7 with a line faired through the data to indicate a reasonable variation with Mach number, the standard error of each point (shown as the vertical lines within the Symbols) being considered.

Comparison with wind-tunnel data.- Wind-tunnel model data corrected for model flexibility effects are given in reference 7 on pages L-124, L-126, and L-128. From these data the wing-fuselage aerodynamic-center data shown in figure 7 (the diamond-shaped symbols) were obtained for the available Mach numbers and may be compared with the flight measurements.

Aerodynamic-center positions at various altitudes.- The wing-fuselage aerodynamic-center position as affected by wing flexibility may be calculated for various altitudes by the use of equation (6), the ΔX_{ac} data of figure 5, and the faired curve of figure 7. The results of these calculations are shown in figure 8 and are considered to be the best estimates of aerodynamic-center position that can be made from the flight data. The results are limited to a low Mach number of 0.40, a high qm_R of 50, and an airplane weight range from 110,000 to 130,000 pounds since these conditions represent the limits within which the flight measurements were obtained.

Zero-Lift Pitching-Moment Coefficient

In the following section the determination of the zero-lift wing-fuselage pitching-moment coefficients from the A coefficient of equation (B2) (for method I) and from the δ_0 coefficient of equation (B5) (for method II) is illustrated with results presented for both methods.

Method I.- Equation (A9) of the appendix is used to determine the wing-fuselage zero-lift pitching-moment coefficient as

$$C_{m_{O_M}} = -\frac{Ax_t}{qS\bar{c}} \tag{10}$$

where

$$x_t = l_t + d \tag{11}$$

For the example maneuver (flight 12, run 27), the substitution into equation (10) of numerical values for A from equation (B4) and

$$x_t = (-552) + (-1.97) = -554 \text{ inches}$$

produces a measured $C_{m_{O_M}}$ value equal to

$$C_{m_{O_M}} = -\frac{(-1702)(-554)}{(159)(1428)(155.9)} = -0.0266$$

The values of $C_{m_{O_M}}$ thus obtained from the A coefficients of table III and the use of equations (10) and (11) are given in table VI and are plotted as a function of Mach number in figure 9 for each of the 68 maneuvers. It was demonstrated in reference 3, however, that the measured tail loads were subject to large zero shifts (ranging from 16,000 to -6,000 pounds). In order to correct the measured zero-lift tail load, use is made of the equation

$$A_{corr} = A - Z' - \frac{Z_T}{x_t} \tag{12}$$

where Z' is the zero shift in measured tail load given in table III of reference 3 for the same maneuvers used in the present analysis and Z_T is the zero shift in tail aerodynamic torque determined from a tail torque and tail angle-of-attack analysis similar to that used for the tail loads in reference 3. For the example maneuver, use of equation (12) gives

$$A_{corr} = -1702 - (20) - (240) = -1962$$

The zero-lift wing-fuselage pitching-moment coefficient is then recalculated by use of the equation

$$C_{m_O} = \frac{-A_{corr}\, x_t}{qS\bar{c}} \tag{13}$$

which with numerical values inserted becomes

$$C_{m_O} = \frac{-(-1962)(-554)}{(159)(222625)} = -0.0307$$

for the example maneuver. The error in C_{m_O} may be estimated by the use of the standard error in the A coefficient as

$$\epsilon C_{m_{O_I}} = \frac{\epsilon_A x_t}{qS\bar{c}} \tag{14}$$

Using the standard error of A from table III gives

$$\epsilon C_{m_{O_I}} = \frac{(\pm 363)(554)}{(159)(222625)} = \pm 0.0057$$

The corrected zero-lift wing-fuselage pitching-moment coefficients and their associated errors are listed in table VI. Figure 10 is a plot of the C_{m_0} values as a function of Mach number and, although scatter does still exist, these results are a decided improvement over the results presented in figure 9.

Method II.- The elevator-angle type of solution may be used to determine the zero-lift wing-fuselage pitching-moment coefficients, as illustrated by equation (A24) of the appendix:

$$C_{m_{0_{II}}} = -\frac{S_t x_t}{S\bar{c}}\left\{\delta_0\left[\left(C_{L_{\alpha_t}}\right)_f \frac{d\alpha_t}{d\delta} + C_{m_\delta}\frac{\bar{c}_t}{x_t}\right] - \left(C_{L_{\alpha_t}}\right)_f\left[3.00 + g\frac{l_t}{V^2}\frac{d\epsilon}{d\alpha} - \left(1 - \frac{d\epsilon}{d\alpha}\right)\left(\alpha_{0_{adj}} + 2.75\right)\right]\right\} \tag{15}$$

The substitution of numerical values for the example maneuver, using the δ_0 value of table IV, geometric parameters, and tail angle-of-attack parameters from reference 3, results in

$$C_{m_{0_{II}}} = -0.0326$$

with an associated error of ±0.0033. Values of $C_{m_{0_{II}}}$ and their standard errors are listed in table VI. Figure 11 is a plot of the $C_{m_{0_{II}}}$ values as a function of Mach number, which is seen to indicate (although with somewhat more scatter) the same average variation with Mach number as illustrated in figure 10 for the method I data.

The correlation between these two methods of evaluating zero-lift wing-fuselage pitching-moment data is seen more clearly in figure 12 where $C_{m_{0_I}}$ is plotted against $C_{m_{0_{II}}}$. The solid line in this figure is the perfect agreement line and the dashed sidebands represent an average departure from agreement based on the average of the errors listed in table VI for each method. With a few exceptions most of the data lie reasonably close to the correlation line.

Variation with Mach number.- The C_{m_0} data of figures 10 and 11 indicated a tendency for the lower altitude data to have smaller absolute values of C_{m_0}. This trend is in agreement with theory since increasing the dynamic pressure at constant Mach number relieves both the bending and torsional moments associated with the zero-lift wing loads and thus reduces the wing contribution to C_{m_0}. Theoretical calculations indicate,

however, that for the maximum qm_R of the present tests the change in C_{m_0} would be only 0.0010. Other factors not specifically corrected for in either set of C_{m_0} data are the pitching-moment coefficient due to tail drag which was estimated to have a maximum value of 0.0023 and the pitching-moment coefficient due to engine thrust which was estimated to vary from 0.0019 to 0.0014 for the dynamic pressure range of the 68 maneuvers used in the analysis.

In order to determine a more definite variation of C_{m_0} with Mach number, the data shown in figures 10 and 11 were used to determine weighted average values of C_{m_0} at each of the Mach number groups shown in table VI. The weights were assigned by use of a weighting factor w similar to that given in equation (7) except that $\epsilon_{X_{ac}}$ was replaced by $\epsilon_{C_{m_0}}$. The weighted average C_{m_0} is given by the equation

$$\overline{C_{m_0}} = \frac{\sum wC_{m_0}}{\sum w} \tag{16}$$

and the standard error of the weighted average is given by the equation

$$\overline{\epsilon_{C_{m_0}}} = \sqrt{\frac{\sum w\left(C_{m_0}\right)^2 - \overline{C_{m_0}} \sum wC_{m_0}}{n \sum w}} \tag{17}$$

The results of the application of equations (16) and (17) to the data for each of the Mach number groups are given in table VI and plotted in figure 13 as a function of Mach number.

Comparison with wind-tunnel data.- Wind-tunnel data corrected for model flexibility effects are given in reference 7 on pages L-124, L-126, and L-128. From these data the wing-fuselage zero-lift pitching-moment coefficients (shown as the diamond symbols in fig. 13) were obtained.

Pitching Moment of Inertia and Radius of Gyration

In the following sections the effects of wing flexibility on the measured and calculated effective airplane moments of inertia are presented.

$k_{y_f}{}^2$ from theory.- The effective moment of inertia of the airplane including the effects of wing flexibility is defined by equation (A10) as

$$I_{y_f} = I_y - d_{\ddot{\theta}} \frac{dL_w}{d\ddot{\theta}} \tag{18}$$

The values of $dL_w/d\ddot{\theta}$ and $d_{\ddot{\theta}}$ to be used in equation (18) are difficult to determine by direct experimentation and recourse is made here to estimating them by theoretical means. The aerodynamic wing load due to pitching acceleration $dL_w/d\ddot{\theta}$ and the associated chordwise center of pressure $d_{\ddot{\theta}}$ were computed by the superposition method of reference 8 as modified and used in references 4 and 5. The results of these computations are shown in figure 14 where the load (in this case for both wings) and the center of pressure (given in terms of percent M.A.C.) are plotted as functions of the flexibility parameter qm_R. The relationship between the ordinate $X_{\ddot{\theta}}$ of figure 14(a) and the center of pressure $d_{\ddot{\theta}}$ is given by the equation

$$d_{\ddot{\theta}} = \left(X_{ac} - X_{\ddot{\theta}}\right)\frac{\bar{c}}{100} \tag{19}$$

where X_{ac} may be found from figure 8. The substitution of equation (19) into equation (18) and division by W/g produces the following equation for effective radius of gyration squared:

$$k_{y_f}{}^2 = k_y{}^2 - \frac{g}{W}\left[\left(X_{ac} - X_{\ddot{\theta}}\right)\frac{\bar{c}}{100}\frac{dL_w}{d\ddot{\theta}}\right] \tag{20}$$

It was found that in the range of interest of qm_R for the present tests the product $\left(X_{ac} - X_{\ddot{\theta}}\right)\frac{dL_w}{d\ddot{\theta}}$ was approximately linear and was equal to

$$\left(X_{ac} - X_{\ddot{\theta}}\right)\frac{dL_w}{d\ddot{\theta}} = 10{,}000qm_R \tag{21}$$

Thus, $k_{y_f}{}^2$ in units of square feet is given by the equation

$$k_{y_f}{}^2 = k_y{}^2 - \frac{32.2 \times 1.559}{12W}10{,}000qm_R$$

$$k_{y_f}{}^2 = k_y{}^2 - 42{,}000\,\frac{qm_R}{W} \tag{22}$$

Values of $k_{y_f}{}^2$ calculated by equation (22) are given in table VII and are plotted in figure 15 as a function of qm_R/W for the 68 test maneuvers. In the calculation of $k_y{}^2$ the empty-weight moment of inertia

given in reference 9 for a ground determination of I_y for the test airplane of 933,000 slug-feet^2 was used along with the fuel weights and locations.

$k_{y_f}{}^2$ from flight data.- The squared values of radius of gyration, obtained by use of method I and method II flight data and equations (A10) and (A26) of the appendix (along with their standard errors), are given in table VII for all maneuvers. The average values of $k_{y_f}{}^2$ (from methods I and II) are also given in table VII and plotted in figure 15. It will be noted that the measured $k_{y_f}{}^2$ values have more scatter but a greater mean variation with qm_R than the calculated values. The disagreement between measured and calculated $k_y{}^2$ values may be due to actual differences in the rigid-wing values or an incorrect theoretical variation with qm_R. In order to allow for these differences, the following procedure was used to correlate flight and calculated values of $k_{y_f}{}^2$. If the values of $k_{y_f}{}^2$ are assumed to be linear with respect to qm_R, the following equations may be written:

$$\left(k_{y_f}{}^2\right)_{calc} = \left(k_y{}^2 + \epsilon_1\right) + \frac{\left(dk_{y_f}{}^2\right)_{calc}}{d\,\frac{qm_R}{W}}\,\frac{qm_R}{W} \tag{23}$$

$$\left(k_{y_f}{}^2\right)_{meas} = \left(k_y{}^2 + \epsilon_2\right) + \frac{\left(dk_{y_f}{}^2\right)_{meas}}{d\,\frac{qm_R}{W}}\,\frac{qm_R}{W} \tag{24}$$

Subtracting equation (23) from equation (24) results in the following equation for $\Delta k_{y_f}{}^2$:

$$\Delta k_{y_f}{}^2 = \left(k_{y_f}{}^2\right)_{meas} - \left(k_{y_f}{}^2\right)_{calc}$$

$$= \left(\epsilon_2 - \epsilon_1\right) + \left[\frac{\left(dk_{y_f}{}^2\right)_{meas}}{d\,\frac{qm_R}{W}} - \frac{\left(dk_{y_f}{}^2\right)_{calc}}{d\,\frac{qm_R}{W}}\right]\frac{qm_R}{W} \tag{25}$$

Equation (25) now permits the correlation of all the data as a function of qm_R since the actual k_y^2 values that differ from run to run because of weight-distribution differences have been eliminated by the subtraction. Columns of $\Delta k_{y_f}^2$ values and $\frac{qm_R}{W}$ are shown in table VII. A least-squares procedure was used with the data to establish the following relationship between $\Delta k_{y_f}^2$ and qm_R/W:

$$\Delta k_{y_f}^2 = (6.6 \pm 5.3) - (11.5 \pm 2.6)\left(\frac{qm_R}{W} \times 10^4\right) \tag{26}$$

Since the standard error of the value $(\epsilon_2 - \epsilon_1)$ of equation (26) is ±5.3 and the average standard error in the measured $k_{y_f}^2$ from table VII is ±5.8, the conclusion to be reached is that the flight measurements agree with the calculated values of k_y^2 for rigid-wing conditions. The difference between the measured and calculated $k_{y_f}^2$ values is in the variation with $\frac{qm_R}{W}$. The equation which represents the flexible-wing effective radius of gyration is, thus, from equations (26), (25), and (22):

$$k_{y_f}^2 = k_y^2 - (115{,}000 \pm 26{,}000 + 42{,}000)\frac{qm_R}{W}$$

or

$$k_{y_f}^2 = k_y^2 - (157{,}000 \pm 26{,}000)\frac{qm_R}{W} \tag{27}$$

$k_{y_f}^2$ from wing-twist data.- The differences between the measured and calculated variations of $k_{y_f}^2$ with qm_R/W were sufficiently large to require some further evidence or confirmation. In figure 15 of reference 2, optigraph measurements for the test airplane were reported which showed a considerable disagreement between measured and calculated values of wing twist associated with pitching accelerations. These twists as plotted in figure 15 of reference 2 are not those due to pitching inertia alone but include an additional air load component. After correction for this component, the aerodynamic load distribution due to twist resulting from pitching inertia was computed by use of the method of reference 10 for the example of figure 15 in reference 2. Integration of the resulting load distribution for both wings gave a load per unit pitching acceleration of -15,040 pounds with a center of pressure at 86.9 percent $\bar{c}$. Both of these points are indicated on the theoretical curves presented in

figure 14. Equation (20) was then used to compute the effective radius of gyration squared as

$$k_{y_f}^2 = 358.35 - \frac{386(1.559)}{144(108,000)}\left[(18.8 - 86.9)(-15,040)\right]$$

$$= 318.52 \text{ feet}^2$$

where 358.35 was the rigid value of k_y^2 and 108,000 was the weight for the conditions of the data of reference 2. The value of qm_R for this example is 19.6; thus, the application of equation (27) results in

$$k_{y_f}^2 = 358.35 - \frac{157,000}{108,000} 19.6$$

$$= 329.86 \text{ feet}^2$$

The theoretical value is determined from equation (22) as 350.73 feet^2.

The following table indicates the correlation between the various methods of determining the effective radius of gyration squared for the test airplane under the average conditions used:

Method	$k_{y_f}^2$, ft^2	$\epsilon k_{y_f}^2$, ft^2
Theoretical (eq. (22))	350.73	-----
Analysis of all 68 flight maneuvers (eq. (27)) . . .	329.86	±4.72
Wing-twist measurements	318.52	-----

Better agreement is seen to exist between the $k_{y_f}^2$ value using wing-twist measurements and the value determined by use of equation (27) than for the theoretical value determined by use of equation (22).

DISCUSSION

The preceding sections of the report have presented the results of the analyses and comparisons with theory and available wind-tunnel data as well as details of the analytical methods used to evaluate the flight

data. The following discussion concerns the importance of the many factors included or omitted in the present analysis.

It is possible to lose sight of the importance of the supporting experimental studies necessary for the analysis of the horizontal-tail loads on a large flexible swept-wing aircraft. Although the present analysis was complicated by some difficulties, which were unforeseen when the flight-test program was originally laid out, the detailed supporting instrumentation which measured airplane angle of attack, wing deflection and twist, and fuselage deflection proved to be invaluable in many phases of the data analysis. In brief, the determination of the rigid wing-fuselage aerodynamic-center position from the flight data was considerably simplified as a result of the flight measurements of wing center of pressure presented in reference 5.

The determination of wing-fuselage zero-lift pitching-moment coefficients from the flight data, which included large zero shifts, was only possible as a result of the tail-load analysis presented in reference 3 which required the wing-lift-curve slope and angle-of-zero-lift data presented in reference 4. A major factor in rationalizing the tail loads as functions of angle of attack and elevator angle was the availability of flight measurements of fuselage deflections which have since been reported in reference 11.

The evaluation of the effects of wing flexibility on the effective moment of inertia was aided by the theoretical studies used in references 1, 2, 4, and 5, the basic moment-of-inertia data provided by reference 9, and the supporting check information obtained from the wing-twist measurements reported in reference 2.

The analysis of elevator-angle-deflection time-history data used in the present report to confirm the direct tail-load evaluation of aerodynamic-center position, zero-lift wing-fuselage pitching-moment coefficient, and effective airplane moment of inertia was based directly on the analysis of references 3 and 4.

Basic-Data Coefficients

When method I was used to fit the tail-load time-history data, it was found that the wing-fuselage pitching moment due to pitching velocity produced immeasurably small horizontal tail loads. A theoretical calculation of the tail load per unit $\frac{\dot{\theta} l_t}{V}$ (as used in the airplane pitching-moment equation (A1), not the tail-load—angle-of-attack equation (A15)) for the example maneuver (flight 12, run 27) resulted in

$$\frac{dL_{t_T}}{d\,\frac{\dot{\theta} l_t}{V}} = -18.0 \text{ pounds per degree}$$

which may be compared with the discarded value of $\frac{dL_{t_T}}{d\,\frac{\dot{\theta} l_t}{V}} = 82$ pounds per degree noted for this maneuver in the flight analysis equation (B3).

The equations used to fit the tail-load and elevator-angle time-history data (eqs. (B2) and (B5)) did not allow for the effects of dynamic wing and fuselage flexibility and, yet, no discernible differences were found in comparing the coefficients of the slow-rate and fast-rate maneuvers. In several cases, dynamic wing-flexibility effects were suspected and the use of wing-tip flapping accelerations improved the fit to the time-history data without altering the primary coefficients. It was felt, therefore, that reasonably accurate results were thus obtained for the bulk of the data analyzed.

A factor somewhat more difficult to define positively is the linearity of the wing-fuselage pitching-moment coefficient with normal-force coefficient. The forms of the equations used force linearity and, for some of the higher altitude data where results were obtained at relatively high normal-force coefficients, this may have resulted in erroneous slopes and intercepts. All suspected departures from linearity were checked by the error-distribution time histories.

Another probable source of error was the sloshing motion of the fuel in the three large unbaffled fuselage fuel tanks, which may have introduced errors in the assumed equation of airplane motion.

Aerodynamic-Center Position

Aside from the factors previously mentioned the accuracy with which the in-flight center-of-gravity position could be determined governs the accuracy of the flight values of wing-fuselage aerodynamic-center position. Corrections were made to account for the effect of airplane attitude on the fuel level and the resultant effect on center-of-gravity position. However, there was some indication from ground tests that the fuel-gage readings were not entirely independent of airplane attitude. The agreement shown between the aerodynamic-center positions determined by methods I and II is excellent and with few exceptions well within their calculated standard errors. The agreement between the data for the rigid-wing aerodynamic-center position shown in figure 7 and the wind-tunnel data seems reasonable. In the Mach number range from 0.70 to 0.775 there is a difference of only $0.01\bar{c}$. The rearward shift of

aerodynamic-center position indicated above a Mach number of about 0.78 is believed to be associated with the fuselage since the wing aerodynamic-center position given in reference 5 remains at roughly 23.4 percent of the local wing chord up to $M = 0.81$.

Zero-Lift Pitching-Moment Coefficient

The agreement between the corrected zero-lift pitching-moment coefficients measured by use of method I and those measured by use of method II indicated that the tail-load zero-shift correction method proposed in reference 3 was theoretically and practically sound. The differences between the flight values of C_{m_0} shown in figure 13 and the wind-tunnel values (ref. 7) are large and not easily explainable.

A source of error in the determination of C_{m_0} from flight data by use of either method I or method II is the accuracy of the elevator-angle measurement. While, for the present tests, the elevator-angle data were repeatable to within ±0.1 degree for comparable flight conditions, an error in C_{m_0} due to elevator-angle zero errors $\left(\epsilon_{C_{m_{0_\delta}}}\right)$ would be approximately equal to

$$\epsilon_{C_{m_{0_\delta}}} \approx 0.68 C_{L_\delta} \epsilon_\delta$$

which with a maximum value of C_{L_δ} from reference 4 as 0.03 would be

$$\epsilon_{C_{m_{0_\delta}}} \approx 0.02 \epsilon_\delta$$

As detailed in the section entitled "Methods and Results," the neglect of the effects of wing twist, tail drag, and pitching moment due to engine thrust could produce a maximum error in the flight measurements of C_{m_0} of +0.0052.

Moment of Inertia and Radius of Gyration

The major factor affecting the accuracy of the determination of I_{y_f} or $k_{y_f}{}^2$ for any individual maneuver is believed to be the effect of fuel sloshing on the airplane motion. In some abrupt maneuvers during which the tail of the airplane accelerated from positive to negative g and back again, the fuel in the rear tank slammed back to the bottom of the tank and, as a result, produced considerable vibration in accelerometer

readings at the center of gravity. Although an attempt was made to eliminate portions of the maneuvers from the analysis when such occurred, the large surging actions of the fuel undoubtedly have contributed to some of the scatter in the I_y data.

The good agreement between the measured and calculated values of k_y^2 for the rigid wing is believed to be indicative of the overall accuracy of the methods used to extract the airplane static stability parameters from the flight tail-load and elevator-angle measurements.

The variation shown between theory and experiment in the changes of $k_{y_f}^2$ with the flexibility parameter qm_R/W is puzzling even though it has been confirmed qualitatively by the wing-twist measurements of reference 2. This disagreement may be associated with unaccounted for local wing-section distortions near the tip or wing twists associated with dynamic motions of the wing tip which may be closely phased with the pitching acceleration time history.

CONCLUDING REMARKS

Flight measurements of wing-fuselage aerodynamic-center position, zero-lift pitching-moment coefficient, and effective airplane moment of inertia have been presented as derived from the analysis of 68 push-pull maneuvers on a large flexible swept-wing airplane in a Mach number range from 0.42 to 0.81 at pressure altitudes from 20,000 to 35,000 feet. The parameters as derived by two methods from measured horizontal-tail loads and elevator angles were in excellent agreement. The method for correcting for tail-load zero shifts (proposed in NACA RM L56J02) was applied to the flight data with good results, as evidenced by a comparison of the uncorrected and corrected zero-lift pitching-moment coefficients derived from the tail-load measurements.

The effects of wing flexibility on the aerodynamic-center position and on the zero-lift pitching-moment coefficient were predictable by theory. The relief provided by the wing bending and twisting due to pitching-acceleration inertia loads to the effective moment of inertia was not predictable by theory. For the one check case available, essential agreement was obtained between optigraph data and tail-load data for the relief due to pitching-acceleration wing loads.

Specifically for the test airplane it was found that:

1. Reasonable agreement was obtained between flight-measured rigid-wing—fuselage aerodynamic-center positions and those determined from wind-tunnel tests.

2. The rigid-wing—fuselage aerodynamic-center position was constant at 24.4 percent mean aerodynamic chord up to a Mach number of 0.78, after which it shifted rearward as the Mach number increased to its maximum flight value of 0.81.

3. The rearward shift in the wing-fuselage aerodynamic center above a Mach number of 0.78 appeared to be associated with the fuselage since the wing aerodynamic-center position given in NACA RM L57E28 remained constant at 23.4 percent of the local wing chord up to a Mach number of 0.81.

4. There were large differences between the wind-tunnel and flight-determined values of zero-lift wing-fuselage pitching-moment coefficient over the complete Mach number range of the tests.

5. The moments of inertia determined from the flight measurements agreed with calculated values for the rigid-wing case.

6. Calculated effective moments of inertia, which included the relief due to wing bending due to pitching-acceleration inertia loads, did not agree with those measured by the present flight tests.

7. For the test airplane, the pitching moment due to pitching-velocity loads on the wing was shown to be insignificant both theoretically and from the tail-load measurements.

Langley Aeronautical Laboratory,
National Advisory Committee for Aeronautics,
Langley Field, Va., August 1, 1957.

APPENDIX A

PITCHING-MOMENT EQUATIONS

The pitching moments on the airplane may be expressed by taking the summation of the moments about the wing-fuselage aerodynamic-center location as

$$\sum M_{ac} = 0 = -nWd + C_{m_0}qS\bar{c} - I_y\ddot{\theta} + L_{\ddot{\theta}}\, d_{\ddot{\theta}}\ddot{\theta} + L_{\dot{\theta}}\, d_{\dot{\theta}}\dot{\theta} + L_t x_t + C_{m_\delta}\delta q S_t \bar{c}_t \tag{A1}$$

In equation (A1) positive forces act upwards, positive moments are nose up, and distances rearward of the aerodynamic center are negative.

The parameters in equation (A1) which are functions of the wing flexibility are the aerodynamic-center location d, the wing-fuselage zero-lift pitching-moment coefficient C_{m_0}, the lift on the wing due to the load induced by wing deflection due to pitching inertia $L_{\ddot{\theta}}$, and the lift on the wing due to the distribution of lift due to pitching velocity $L_{\dot{\theta}}$. The term $L_{\ddot{\theta}}$ is defined as

$$L_{\ddot{\theta}} = \frac{dL_w}{d\ddot{\theta}}\ddot{\theta} \tag{A2}$$

and the term $L_{\dot{\theta}}$ is defined as

$$L_{\dot{\theta}} = \frac{dL_w}{d\,\dfrac{\dot{\theta}l_t}{V}}\,\frac{\dot{\theta}l_t}{V} \tag{A3}$$

Method I - Direct Tail-Load Measurement

Equation (A1) may be written as

$$L_t x_t + C_{m_\delta}\delta q S_t \bar{c}_t = -C_{m_0}qS\bar{c} + nWd + \left(I_y - \frac{dL_w}{d\ddot{\theta}}\, d_{\ddot{\theta}}\right)\ddot{\theta} - \frac{dL_w}{d\,\dfrac{\dot{\theta}l_t}{V}}\, d_{\dot{\theta}}\,\frac{\dot{\theta}l_t}{V} \tag{A4}$$

For the test data analyzed in the present report, the horizontal-tail aerodynamic load L_t and the tail aerodynamic torque

$$T_t = C_{m_\delta} \delta q S_t \bar{c}_t \tag{A5}$$

were both measured by means of strain gages; thus, equation (A4) may be used as

$$L_{t_T} = L_t + \frac{T_t}{x_t} = \frac{-C_{m_0} q S \bar{c}}{x_t} + \frac{nWd}{x_t} + \left(I_y - \frac{dL_w}{d\ddot{\theta}} d_{\ddot{\theta}}\right) \frac{\ddot{\theta}}{x_t} - \frac{dL_w}{d \frac{\dot{\theta} l_t}{V}} \frac{d_{\dot{\theta}}}{x_t} \frac{\dot{\theta} l_t}{V} \tag{A6}$$

In a form simplified for least-squares analysis, equation (A6) may be written as

$$L_{t_T} = A + Bn + C\ddot{\theta} + D \frac{\dot{\theta} l_t}{V} \tag{A7}$$

From the coefficients A, B, C, and D of equation (A7) and the corresponding terms of equation (A6), the pitching-moment parameters of interest may be defined as aerodynamic-center location d

$$d = \frac{B l_t}{W - B} \tag{A8}$$

zero-lift pitching-moment coefficient C_{m_0}

$$C_{m_0} = -\frac{A x_t}{q S \bar{c}} \tag{A9}$$

effective airplane moment of inertia I_{y_f}

$$I_{y_f} = I_y - \frac{dL_w}{d\ddot{\theta}} d_{\ddot{\theta}} = C x_t \tag{A10}$$

and the pitching moment due to pitching velocity $L_{\dot{\theta}} d_{\dot{\theta}}$

$$L_{\dot{\theta}} d_{\dot{\theta}} = D \frac{\dot{\theta} l_t}{V} x_t \tag{A11}$$

Method II - Pitching-Moment Parameters From

Elevator-Angle Measurements

For the determination of pitching-moment parameters from elevator-angle measurements, a more complicated series of equations must be written which also include the effect of fuselage deflection on the horizontal-tail angle of attack. Equation (A1) is rewritten as

$$L_t = -C_{m_0} \frac{qS\bar{c}}{x_t} + \frac{nWd}{x_t} + \left(\frac{I_y}{x_t} - \frac{dL_w}{d\ddot{\theta}} \frac{d\ddot{\theta}}{x_t}\right)\ddot{\theta} - \left(\frac{C_{m_\delta} \delta q S_t \bar{c}_t}{x_t}\right) - \frac{dL_w}{d\,\frac{\dot{\theta} l_t}{V}} \frac{d\dot{\theta}}{x_t} \frac{\dot{\theta} l_t}{V} \tag{A12}$$

Now

$$L_t = C_{L_{\alpha_t}} q S_t \alpha_t \tag{A13}$$

and α_t can be written specifically for the test airplane by using equations (4) and (6) of reference 3:

$$\alpha_t = -3.00 + \alpha_w\left(1 - \frac{d\epsilon}{d\alpha}\right) - \frac{\dot{\theta} l_t}{V} \frac{d\epsilon}{d\alpha} + g \frac{(n - 1)}{V^2} l_t \frac{d\epsilon}{d\alpha} - \frac{\dot{\theta} l_t}{V} +$$

$$\frac{d\alpha_t}{d\delta} \delta + \frac{di_t}{dn_t} n_t + \frac{di_t}{dL_t} L_t \tag{A14}$$

By the substitution of equation (A14) into (A13) and factoring out the tail-load terms, the tail-load equation may be rewritten as

$$L_t = \frac{C_{L_{\alpha_t}} q S_t}{1 - \frac{di_t}{dL_t} C_{L_{\alpha_t}} q S_t}\left[-3.00 + \alpha_w\left(1 - \frac{d\epsilon}{d\alpha}\right) + \frac{d\alpha_t}{d\delta} \delta - \frac{\dot{\theta} l_t}{V}\left(1 + \frac{d\epsilon}{d\alpha}\right) +\right.$$

$$\left. g \frac{l_t}{V^2} \frac{d\epsilon}{d\alpha}(n - 1) + \frac{di_t}{dn_t} n_t\right] \tag{A15}$$

Hereafter, the expression $\dfrac{C_{L_{\alpha_t}}}{1 - \frac{di_t}{dL_t} C_{L_{\alpha_t}} q S_t}$ is defined as the effective tail-lift-curve slope $\left(C_{L_{\alpha_t}}\right)_f$.

With the use of the additional equations

$$n_t = n - 1.352\ddot{\theta} \tag{A16}$$

$$\alpha_w = \alpha_{0_{adj}} + \frac{1}{a_F} C_{N_{A_C}} + i_w \tag{A17}$$

$$C_{N_{A_C}} = \frac{nW}{qS} - \frac{I_{y_f}\ddot{\theta}}{x_t S q} \tag{A18}$$

where equation (A16) is the tail load factor expressed in terms of the center-of-gravity normal load factor and pitching acceleration and equations (A17) and (A18) are used in reference 3 to define the wing angle of attack, equations (A15) and (A12) can be combined to give

$$\delta = \delta_0 + \frac{\partial\delta}{\partial \frac{\dot{\theta} l_t}{V}} \frac{\dot{\theta} l_t}{V} + \frac{\partial\delta}{\partial n} n + \frac{\partial\delta}{\partial\ddot{\theta}} \ddot{\theta} \tag{A19}$$

where

$$\frac{\partial\delta}{\partial \frac{\dot{\theta} l_t}{V}} = \frac{\left[\left(1 + \frac{d\epsilon}{d\alpha}\right)\left(C_{L_{\alpha_t}}\right)_f - \frac{dL_w}{d\frac{\dot{\theta} l_t}{V}} \frac{d\dot{\theta}}{x_t q S_t}\right]}{\left[\left(C_{L_{\alpha_t}}\right)_f \frac{d\alpha_t}{d\delta} + C_{m_\delta} \frac{\bar{c}_t}{x_t}\right]} \tag{A20}$$

$$\delta_0 = \frac{-C_{m_0} \frac{S\bar{c}}{S_t x_t} + \left(3.00 + g \frac{l_t}{V^2} \frac{d\epsilon}{d\alpha}\right)\left(C_{L_{\alpha_t}}\right)_f - \left(1 - \frac{d\epsilon}{d\alpha}\right)\left(C_{L_{\alpha_t}}\right)_f \left(\alpha_{0_{adj}} + i_w\right)}{\left[\left(C_{L_{\alpha_t}}\right)_f \frac{d\alpha_t}{d\delta} + C_{m_\delta} \frac{\bar{c}_t}{x_t}\right]} \tag{A21}$$

$$\frac{\partial\delta}{\partial n} = \frac{\left[\frac{Wd}{qS_t x_t} - \frac{di_t}{dn_t}\left(C_{L_{\alpha_t}}\right)_f - g \frac{l_t}{V^2} \frac{d\epsilon}{d\alpha}\left(C_{L_{\alpha_t}}\right)_f - \left(1 - \frac{d\epsilon}{d\alpha}\right)\left(C_{L_{\alpha_t}}\right)_f \frac{W}{a_F q S}\right]}{\left[\left(C_{L_{\alpha_t}}\right)_f \frac{d\alpha_t}{d\delta} + C_{m_\delta} \frac{\bar{c}_t}{x_t}\right]} \tag{A22}$$

and

$$\frac{\partial\delta}{\partial\ddot{\theta}} = \frac{\dfrac{I_{y_f}}{qS_t x_t} + 1.352\left(C_{l_{\alpha_t}}\right)_f \dfrac{di_t}{dn_t} + \left(1 - \dfrac{d\epsilon}{d\alpha}\right)\dfrac{\left(C_{L_{\alpha_t}}\right)_f I_{y_f}}{a_F x_t Sq}}{\left[\left(C_{L_{\alpha_t}}\right)_f \dfrac{d\alpha_t}{d\delta} + C_{m_\delta}\dfrac{\bar{c}_t}{x_t}\right]} \tag{A23}$$

From equation (A21) the zero-lift pitching-moment coefficient C_{m_0} may be derived as

$$C_{m_0} = -\frac{S_t x_t}{S\bar{c}}\left\{\delta_0\left[\left(C_{L_{\alpha_t}}\right)_f \frac{d\alpha_t}{d\delta} + C_{m_\delta}\frac{\bar{c}_t}{x_t}\right] - \left(C_{L_{\alpha_t}}\right)_f\left[3.00 + g\frac{l_t}{V^2}\frac{d\epsilon}{d\alpha} - \left(1 - \frac{d\epsilon}{d\alpha}\right)\left(\alpha_{0_{adj}} + 2.75\right)\right]\right\} \tag{A24}$$

The aerodynamic-center location d may be derived from equation (A22) as

$$d = \frac{l_t\left(C_{L_{\alpha_t}}\right)_f\left[\dfrac{\partial\delta}{\partial n}\dfrac{d\alpha_t}{d\delta} + \dfrac{di_t}{dn_t} + g\dfrac{l_t}{V^2}\dfrac{d\epsilon}{d\alpha} + \left(1 - \dfrac{d\epsilon}{d\alpha}\right)\dfrac{W}{a_F qS}\right] + \dfrac{\partial\delta}{\partial n}C_{m_\delta}\bar{c}_t}{\dfrac{W}{qS_t} - \left(C_{L_{\alpha_t}}\right)_f\left[\dfrac{\partial\delta}{\partial n}\dfrac{d\alpha_t}{d\delta} + \dfrac{di_t}{dn_t} + g\dfrac{l_t}{V^2}\dfrac{d\epsilon}{d\alpha} + \left(1 - \dfrac{d\epsilon}{d\alpha}\right)\dfrac{W}{a_F qS}\right]} \tag{A25}$$

and the effective moment of inertia I_{y_f}, from equation (A23) as

$$I_{y_f} = \frac{qS_t x_t}{1 + \left(1 - \dfrac{d\epsilon}{d\alpha}\right)\dfrac{S_t\left(C_{L_{\alpha_t}}\right)_f}{Sa_F}}\left\{\frac{\partial\delta}{\partial\ddot{\theta}}\left[\left(C_{l_{\alpha_t}}\right)_f \frac{d\alpha_t}{d\delta} + C_{m_\delta}\frac{\bar{c}_t}{x_t}\right] - 1.352\left(C_{l_{\alpha_t}}\right)_f \frac{di_t}{dn_t}\right\} \tag{A26}$$

APPENDIX B

ANALYSIS OF BASIC DATA

As shown in appendix A the wing-fuselage aerodynamic-center position, zero-lift wing-fuselage pitching-moment coefficient, and effective moment of inertia may be determined from the coefficients of equations (A7) and (A19). The following sections give the least-squares procedures used for the determination of these coefficients and illustrative examples for both methods I and II.

Solutions by Use of Method I

For analysis of flight tail-load measurements for each maneuver, equations of the form of equation (A7) may be solved for the coefficients A, B, C, and D as follows:

$$\begin{Bmatrix} A \\ B \\ C \\ D \end{Bmatrix} = \left[\begin{Vmatrix} 1 & n & \ddot{\theta} & \dot{\theta} l_t/V \\ \cdot & \cdot & \cdot & \cdot \\ \cdot & \cdot & \cdot & \cdot \\ \cdot & \cdot & \cdot & \cdot \\ \cdot & \cdot & \cdot & \cdot \\ \cdot & \cdot & \cdot & \cdot \\ \cdot & \cdot & \cdot & \cdot \end{Vmatrix}^T \begin{Vmatrix} 1 & n & \ddot{\theta} & \dot{\theta} l_t/V \\ \cdot & \cdot & \cdot & \cdot \\ \cdot & \cdot & \cdot & \cdot \\ \cdot & \cdot & \cdot & \cdot \\ \cdot & \cdot & \cdot & \cdot \\ \cdot & \cdot & \cdot & \cdot \\ \cdot & \cdot & \cdot & \cdot \end{Vmatrix} \right]^{-1} \begin{Vmatrix} 1 & n & \ddot{\theta} & \dot{\theta} l_t/V \\ \cdot & \cdot & \cdot & \cdot \\ \cdot & \cdot & \cdot & \cdot \\ \cdot & \cdot & \cdot & \cdot \\ \cdot & \cdot & \cdot & \cdot \\ \cdot & \cdot & \cdot & \cdot \\ \cdot & \cdot & \cdot & \cdot \end{Vmatrix}^T \begin{Bmatrix} L_{t_T} \\ \cdot \\ \cdot \\ \cdot \\ \cdot \\ \cdot \\ \cdot \end{Bmatrix} \tag{B1}$$

In equation (B1) the individual rows of the rectangular matrix and the column matrix L_{t_T} represent simultaneous measurements of the indicated parameters at each of various times in a given push-pull maneuver. Equation (B1) in the following equivalent form was used for the determination of the A, B, C, and D coefficients for each of the 68 maneuvers listed in table II:

$$\begin{Bmatrix} A \\ B \\ C \\ D \end{Bmatrix} = \begin{bmatrix} N & \sum n & \sum \ddot{\theta} & \sum \dot{\theta} l_t/V \\ \sum n & \sum n^2 & \sum \ddot{\theta} n & \sum \left(\dot{\theta} l_t/V\right) n \\ \sum \ddot{\theta} & \sum n\ddot{\theta} & \sum \ddot{\theta}^2 & \sum \left(\dot{\theta} l_t/V\right)\ddot{\theta} \\ \sum \dot{\theta} l_t/V & \sum n\left(\dot{\theta} l_t/V\right) & \sum \ddot{\theta}\left(\dot{\theta} l_t/V\right) & \sum \left(\dot{\theta} l_t/V\right)^2 \end{bmatrix}^{-1} \begin{Bmatrix} \sum L_{t_T} \\ \sum L_{t_T} n \\ \sum L_{t_T}\ddot{\theta} \\ \sum L_{t_T}\left(\dot{\theta} l_t/V\right) \end{Bmatrix} \tag{B2}$$

The determination of the A, B, C, and D coefficients for each maneuver by the use of equation (B2) requires time-history measurements of the following quantities:

n normal load factor at center of gravity

$\ddot{\theta}$ pitching acceleration at center of gravity

$\dot{\theta} l_t/V$ tail angle of attack due to pitching velocity

L_{t_T} aerodynamic tail load plus tail aerodynamic pitching moment

Figures 2 and 3 illustrate in time-history form the data used in the analysis of a typical maneuver (flight 12, run 27). The pitching acceleration $\ddot{\theta}$ has been corrected for instrument frequency-response characteristics.

The use of equation (B2) with the time-history data of figures 2 and 3 resulted in the following equation for tail load for this maneuver:

$$L_{t_T} = -1722 + 497n - 24150\ddot{\theta} + 82\dot{\theta} l_t/V \tag{B3}$$

The coefficient of $\dot{\theta} l_t/V$ was small in comparison with its standard error and the fit to the time history was not improved by the inclusion of this pitching-velocity parameter. Analysis of the other maneuvers also indicated that the parameter $\dot{\theta} l_t/V$ did not contribute significantly to the pitching-moment tail-load equation. Thus, for this and subsequent maneuvers the A, B, and C coefficients to be presented were obtained

by using equations of the form of equation (B2) with the $\dot{\theta} l_t/V$ term omitted. With the pitching-velocity term omitted, the equation determined as fitting the time history of L_{t_T} for flight 12, run 27 became

$$L_{t_T} = -1702 + 392n - 24059\ddot{\theta} \tag{B4}$$

The calculated tail load L_{t_T} (eq. (B4)) is compared in figure 3 with the measured time history from which it was derived. The fit is reasonably good and this sample maneuver is representative of the worst rather than the best correlation obtained.

The A, B, and C coefficients obtained from the least-squares analysis of each of the 68 maneuvers are given in table III. Also listed in the table are the standard errors of fit and the standard errors of the individual coefficients.

Solutions by Use of Method II

The elevator-angle equation (eq. (A19)) may be written in a form for least-squares solution of time-history data as follows:

$$\begin{Bmatrix} \delta_0 \\ \frac{\partial\delta}{\partial n} \\ \frac{\partial\delta}{\partial\ddot{\theta}} \\ \frac{\partial\delta}{\partial\dot{\theta} l_t/V} \end{Bmatrix} = \begin{bmatrix} N & \sum n & \sum \ddot{\theta} & \sum \dot{\theta} l_t/V \\ \sum n & \sum n^2 & \sum \ddot{\theta} n & \sum (\dot{\theta} l_t/V)n \\ \sum \ddot{\theta} & \sum n\ddot{\theta} & \sum \ddot{\theta}^2 & \sum (\dot{\theta} l_t/V)\ddot{\theta} \\ \sum \dot{\theta} l_t/V & \sum n(\dot{\theta} l_t/V) & \sum \ddot{\theta}(\dot{\theta} l_t/V) & \sum (\dot{\theta} l_t/V)^2 \end{bmatrix}^{-1} \begin{Bmatrix} \sum \delta \\ \sum \delta n \\ \sum \delta\ddot{\theta} \\ \sum \delta(\dot{\theta} l_t/V) \end{Bmatrix} \tag{B5}$$

In figure 4 the elevator angle is shown in time-history form for the example maneuver (flight 12, run 27). When the elevator-angle data are used in addition to the data shown in figure 3, the following equation is obtained by solution of equation (B5):

$$\delta = 4.548 + 3.534 \frac{\dot{\theta} l_t}{V} - 6.620n - 21.563\ddot{\theta} \tag{B6}$$

In this case the term $\dot{\theta} l_t/V$ is an important parameter and is retained for all solutions. A time history of the elevator angles computed by use of equation (B6) is shown in figure 4. The agreement is reasonably good but again the example maneuver is not as good a fit as was obtained with the majority of the maneuvers analyzed.

The elevator-angle coefficients of equation (B5) for all 68 maneuvers are listed in table IV along with their standard errors and errors of fit.

REFERENCES

1. Mayo, Alton P., and Ward, John F.: Experimental Influence Coefficients for the Deflection of the Wing of a Full-Scale, Swept-Wing Bomber. NACA RM L53L23, 1954.

2. Mayo, Alton P., and Ward, John F.: Flight Investigation and Analysis of the Wing Deformations of a Swept-Wing Bomber During Push-Pull Maneuvers. NACA RM L54K24a, 1955.

3. Aiken, William S., Jr., and Fisher, Raymond A.: Horizontal-Tail Parameters As Determined From Flight-Test Tail Loads on a Flexible Swept-Wing Jet Bomber. NACA RM L56J02, 1957.

4. Aiken, William S., Jr., and Fisher, Raymond A.: Lift-Curve Slopes Determined in Flight on a Flexible Swept-Wing Jet Bomber. NACA RM L56E21a, 1956.

5. Gainer, Patrick A., and Harper, Paul W.: Analysis of Wing Loads Measured on a Flexible Swept-Wing Jet Bomber During Push-Pull Maneuvers. NACA RM L57E28, 1957.

6. Skopinski, T. H., Aiken, William S., Jr., and Huston, Wilber B.: Calibration of Strain-Gage Installations in Aircraft Structures for the Measurement of Flight Loads. NACA Rep. 1178, 1954. (Supersedes NACA TN 2993.)

7. Budish, Nathan N.: Longitudinal Stability at High Airspeeds. Doc. No. D-8603-0 (Contract No. W33-038 ac-22413), Boeing Airplane Co., Feb. 29, 1952.

8. Brown, R. B., Holtby, K. F., and Martin, H. C.: A Superposition Method for Calculating the Aeroelastic Behavior of Swept Wings. Jour. Aero. Sci., vol. 18, no. 8, Aug. 1951, pp. 531-542.

9. Cole, Henry A., Jr., and Bennion, Frances L.: Measurement of the Longitudinal Moment of Inertia of a Flexible Airplane. NACA TN 3870, 1956. (Supersedes NACA RM A55J21.)

10. Gray, W. L., and Schenk, K. M.: A Method for Calculating the Subsonic Steady-State Loading on an Airplane With a Wing of Arbitrary Plan Form and Stiffness. NACA TN 3030, 1953.

11. Mayo, Alton P.: Flight Investigation and Theoretical Calculations of the Fuselage Deformations of a Swept-Wing Bomber During Push-Pull Maneuvers. NACA RM L56L05, 1957.

TABLE I.- AIRPLANE CHARACTERISTICS AND DIMENSIONS

Horizontal tail:	
Total area, sq ft	268
Span, ft	33
Root chord, ft	11.42
Mean aerodynamic chord, ft	8.58
Distance from horizontal-tail 25 percent M.A.C. to wing 25 percent M.A.C., ft	46.52
Incidence angle, deg	-0.25
Sweepback (25-percent-chord line), deg	32.9
Aspect ratio	4.06
Taper ratio	0.423
Airfoil section	BAC 100
Strain-gage reference station (percent semispan)	5.3
Wing:	
Total area, sq ft	1,428
Span, ft	116
Mean aerodynamic chord, in.	155.9
Aspect ratio	9.42
Taper ratio	0.420
Incidence angle, deg	2.75
Sweepback (25-percent-chord line), deg	35
Airfoil section	BAC 145

TABLE II.- SUMMARY OF FLIGHT CONDITIONS

Flight	Run	$\bar{M}$	$\bar{q}$, lb/sq ft	Pressure altitude, ft	W, lb	Center-of-gravity location, percent M.A.C.
2	27	0.636 ± 0.002	137 ± 2	35,200	112,600	22.2
	28	0.735 ± 0.001	184 ± 1	34,900	112,300	21.8
	29	0.796 ± 0.004	216 ± 2	34,800	112,200	21.7
3	11	0.750 ± 0.001	196 ± 1	34,600	120,300	14.1
	12	0.728 ± 0.007	188 ± 5	34,100	120,100	14.2
	13	0.689 ± 0.006	167 ± 3	34,400	119,900	14.3
	14	0.631 ± 0.002	140 ± 1	34,600	119,000	14.5
4	19	0.699 ± 0.002	264 ± 3	25,000	108,900	21.2
	20	0.591 ± 0.001	190 ± 1	25,000	108,700	21.5
	21	0.486 ± 0.003	128 ± 1	25,300	108,400	22.1
6	11	0.789 ± 0.001	264 ± 3	30,800	108,800	13.3
	12	0.790 ± 0.001	268 ± 1	30,500	108,700	13.3
	13	0.741 ± 0.001	244 ± 1	29,800	108,400	13.3
	14	0.690 ± 0.001	215 ± 1	29,400	108,200	13.6
	15	0.643 ± 0.003	187 ± 2	29,400	107,600	13.6
8	4	0.544 ± 0.008	163 ± 4	24,900	124,800	23.6
	5	0.648 ± 0.004	233 ± 3	24,800	124,500	23.3
	6	0.758 ± 0.002	314 ± 4	25,100	124,000	23.3
9	1	0.598 ± 0.003	125 ± 1	34,800	126,700	24.1
	2	0.647 ± 0.004	147 ± 2	34,900	126,200	23.7
	3	0.681 ± 0.001	161 ± 1	35,200	126,100	23.7
	4	0.731 ± 0.003	185 ± 1	35,200	125,700	23.6
	5	0.779 ± 0.002	214 ± 1	34,900	125,400	23.4
	6	0.795 ± 0.001	216 ± 1	35,500	125,200	23.7
	7	0.810 ± 0	225 ± 1	35,300	124,900	23.9
10	3	0.598 ± 0.003	159 ± 2	29,800	127,200	23.7
	4	0.647 ± 0.001	185 ± 0	29,900	126,500	23.1
	5	0.681 ± 0.001	200 ± 1	30,500	126,300	23.1
	6	0.726 ± 0.001	230 ± 1	30,200	126,100	23.0
	7	0.763 ± 0	254 ± 0	30,200	125,400	23.2
	8	0.789 ± 0.001	260 ± 1	31,100	125,200	23.4
	9	0.812 ± 0.001	274 ± 1	31,300	124,900	23.5
11	11	0.495 ± 0.003	138 ± 1	24,400	109,200	23.0
	12	0.542 ± 0.003	164 ± 1	24,600	108,900	22.5
	13	0.597 ± 0.001	194 ± 1	25,100	108,500	22.3
	14	0.636 ± 0	222 ± 0	25,000	108,500	22.2
	15	0.681 ± 0	247 ± 0	25,700	108,400	22.4
	16	0.702 ± 0.001	266 ± 1	25,400	107,800	21.9
	17	0.734 ± 0	291 ± 0	25,300	107,500	21.9
	24	0.427 ± 0.001	126 ± 1	19,700	103,700	23.8
12	6	0.584 ± 0.001	127 ± 1	33,700	120,400	15.9
	7	0.642 ± 0.001	147 ± 1	34,400	120,300	15.7
	8	0.679 ± 0.001	162 ± 0	34,900	119,900	15.5
	9	0.721 ± 0.001	178 ± 1	35,300	119,600	15.2
	10	0.773 ± 0.001	202 ± 1	35,400	119,100	15.2
	11	0.790 ± 0	215 ± 0	35,200	118,800	14.9
	12	0.812 ± 0	228 ± 0	35,200	118,700	14.7
	17	0.483 ± 0.001	130 ± 1	24,600	116,600	15.3
	18	0.532 ± 0	157 ± 0	24,700	116,500	14.8
	19	0.600 ± 0.001	198 ± 1	24,900	116,400	14.3
	20	0.637 ± 0	223 ± 0	25,000	116,300	14.3
	21	0.682 ± 0.001	255 ± 1	25,000	116,100	14.5
	22	0.694 ± 0.001	262 ± 0	25,200	115,800	14.3
	23	0.735 ± 0.001	298 ± 1	24,900	115,400	14.4
	24	0.642 ± 0.002	279 ± 3	20,000	111,100	21.7
	25	0.595 ± 0.002	242 ± 1	19,800	111,100	21.8
	26	0.543 ± 0	202 ± 1	19,700	110,600	22.2
	27	0.482 ± 0.002	159 ± 1	19,700	110,300	22.9
	28	0.427 ± 0.001	126 ± 1	19,600	110,200	23.1
16	1	0.642 ± 0.001	282 ± 1	19,900	117,100	14.8
	2	0.599 ± 0.002	246 ± 2	19,800	116,800	14.7
	3	0.542 ± 0.002	200 ± 2	20,000	116,600	14.2
	4	0.482 ± 0.002	160 ± 1	19,800	116,000	14.9
	5	0.428 ± 0.003	127 ± 2	19,500	115,500	15.2
	6	0.433 ± 0.002	131 ± 2	19,300	115,100	14.9
17	5	0.808 ± 0.001	364 ± 1	24,600	116,400	14.1
	6	0.762 ± 0	326 ± 0	24,500	116,200	14.2
	7	0.725 ± 0	295 ± 0	24,500	115,600	14.1

TABLE III.- MEASURED TAIL-LOAD COEFFICIENTS OBTAINED BY USE OF EQUATION (B2)

Flight	Run	A	ϵ_A	B	ϵ_B	C	ϵ_C	Standard error
2	27	-1,264	±184	279	±180	-30,725	±980	104
	28	-4,207	±288	920	±180	-28,944	±861	122
	29	-6,553	±312	776	±121	-29,533	±811	78
3	11	-2,143	±207	-1,260	±149	-29,823	±849	95
	12	-1,627	±99	-1,446	±84	-31,656	±611	123
	13	-799	±93	-1,420	±76	-30,567	±722	89
	14	385	±81	-1,575	±106	-31,408	±578	69
4	19	-6,451	±191	1,108	±77	-24,466	±424	69
	20	-4,272	±206	691	±133	-24,964	±500	95
	21	-1,181	±185	91	±202	-26,844	±625	94
6	11	-3,782	±123	-1,558	±101	-26,492	±626	85
	12	-4,543	±214	-1,016	±92	-22,263	±485	76
	13	-3,352	±357	-1,305	±211	-23,929	±755	146
	14	-2,062	±343	-1,610	±229	-26,189	±984	141
	15	-1,494	±242	-1,286	±182	-24,484	±793	105
8	4	8,375	±292	1,302	±111	-27,745	±743	69
	5	6,254	±132	1,805	±99	-27,986	±460	101
	6	2,096	±50	2,238	±88	-26,878	±411	89
9	1	14,921	±352	1,259	±144	-31,453	±533	91
	2	12,383	±597	1,553	±121	-30,431	±1,012	110
	3	10,074	±338	1,526	±114	-30,379	±670	73
	4	7,494	±217	1,948	±144	-28,856	±493	98
	5	3,910	±125	2,073	±79	-27,788	±461	89
	6	2,723	±190	1,418	±211	-30,925	±1,204	108
	7	1,815	±187	1,000	±205	-30,484	±1,321	91
10	3	11,828	±326	988	±218	-30,098	±727	153
	4	9,410	±281	1,091	±285	-32,209	±875	203
	5	7,705	±200	1,124	±262	-29,850	±686	128
	6	3,218	±84	1,775	±136	-28,107	±416	98
	7	1,170	±106	1,554	±168	-29,071	±536	87
	8	-673	±296	1,807	±381	-27,558	±960	182
	9	-1,116	±126	1,379	±130	-28,669	±487	106
11	11	362	±386	164	±507	-26,600	±953	295
	12	-532	±155	417	±183	-26,567	±553	146
	13	-1,650	±104	669	±104	-26,062	±406	89
	14	-3,797	±209	1,057	±156	-24,022	±521	161
	15	-4,566	±263	1,009	±171	-24,700	±624	210
	16	-5,821	±221	1,257	±142	-23,845	±406	148
	17	-7,315	±267	1,382	±143	-22,164	±416	124
	24	-257	±286	501	±216	-26,232	±1,263	108
12	6	6,965	±216	-716	±320	-26,798	±598	180
	7	5,332	±259	-378	±363	-25,781	±683	284
	8	4,988	±473	-1,873	±658	-27,161	±943	280
	9	2,387	±203	-592	±297	-25,096	±607	279
	10	-286	±697	-715	±874	-23,892	±1,313	480
	11	-1,028	±656	-1,022	±750	-24,865	±1,268	366
	12	-2,766	±679	-1,283	±456	-24,518	±838	169
	17	-4,802	±512	-1,450	±395	-26,425	±642	222
	18	-5,436	±338	-1,588	±244	-26,273	±467	152
	19	-7,554	±309	-604	±165	-24,821	±377	191
	20	-8,431	±402	-650	±217	-24,479	±474	186
	21	-9,518	±432	-651	±226	-24,257	±491	155
	22	-9,504	±510	-538	±256	-23,682	±581	211
	23	-10,676	±321	-263	±135	-23,659	±346	130
	24	-7,060	±305	1,338	±184	-22,970	±440	158
	25	-5,765	±259	1,027	±173	-23,239	±380	163
	26	-3,765	±166	842	±128	-24,437	±354	115
	27	-1,702	±363	392	±358	-24,059	±637	267
	28	-880	±461	401	±478	-24,726	±821	289
16	1	2,268	±80	-824	±114	-26,414	±347	90
	2	2,367	±138	-870	±158	-25,959	±454	135
	3	3,050	±141	-1,263	±169	-27,119	±557	117
	4	3,202	±134	-1,467	±161	-27,302	±496	90
	5	3,588	±97	-1,973	±113	-28,371	±419	71
	6	2,789	±69	-1,677	±80	-27,929	±242	70
17	5	-5,376	±246	-166	±126	-22,942	±457	135
	6	-3,392	±272	-384	±188	-24,246	±561	221
	7	-1,383	±436	-1,260	±393	-26,152	±932	225

TABLE IV.- MEASURED ELEVATOR-ANGLE COEFFICIENTS OBTAINED BY USE OF EQUATION (B5)

Flight	Run	δ_0	ϵ_{δ_0}	$\frac{\partial\delta}{\partial\frac{\dot{\theta}l_t}{V}}$	$\epsilon_{\partial\delta/\partial(\dot{\theta}l_t/V)}$	$\frac{\partial\delta}{\partial n}$	$\epsilon_{\partial\delta/\partial n}$	$\frac{\partial\delta}{\partial\ddot{\theta}}$	$\epsilon_{\partial\delta/\partial\ddot{\theta}}$	Standard error
2	27	3.502	±0.125	4.648	±0.163	-6.514	±0.145	-27.369	±0.244	0.077
	28	3.456	±.145	4.606	±.276	-4.467	±.150	-19.595	±.240	.099
	29	3.114	±.078	5.282	±.233	-3.357	±.085	-15.547	±.183	.048
3	11	3.105	±.157	4.573	±.244	-6.123	±.186	-19.835	±.270	.068
	12	3.408	±.124	3.500	±.371	-6.680	±.144	-22.237	±.157	.137
	13	3.397	±.127	4.013	±.289	-7.672	±.132	-23.061	±.324	.111
	14	3.895	±.111	3.212	±.159	-9.815	±.146	-31.507	±.232	.072
4	19	4.130	±.061	4.031	±.173	-3.995	±.065	-14.042	±.220	.055
	20	4.074	±.151	3.599	±.190	-5.763	±.162	-19.839	±.200	.106
	21	4.055	±.273	3.251	±.185	-8.062	±.339	-27.583	±.318	.112
6	11	3.219	±.067	4.848	±.225	-4.303	±.074	-12.627	±.121	.047
	12	3.225	±.098	4.881	±.216	-4.279	±.099	-12.335	±.132	.060
	13	3.447	±.153	4.101	±.191	-4.768	±.150	-13.523	±.145	.083
	14	3.827	±.190	4.080	±.243	-5.876	±.192	-17.037	±.212	.089
	15	3.484	±.234	3.862	±.252	-6.426	±.254	-18.269	±.286	.106
8	4	3.553	±.108	3.321	±.186	-6.334	±.119	-22.399	±.270	.063
	5	4.232	±.063	3.829	±.135	-4.597	±.063	-17.372	±.110	.070
	6	3.945	±.035	4.700	±.102	-3.163	±.037	-12.170	±.073	.045
9	1	2.641	±.177	3.936	±.164	-7.225	±.224	-30.945	±.306	.108
	2	3.491	±.249	3.702	±.204	-6.594	±.308	-25.691	±.390	.082
	3	3.564	±.094	4.362	±.156	-5.625	±.111	-21.500	±.271	.066
	4	3.074	±.192	3.724	±.284	-4.570	±.232	-20.438	±.328	.088
	5	2.960	±.089	4.387	±.170	-3.304	±.076	-17.589	±.166	.101
	6	3.157	±.147	4.682	±.309	-3.398	±.178	-17.349	±.324	.080
	7	3.335	±.245	5.067	±.465	-3.630	±.311	-17.199	±.535	.109
10	3	3.494	±.142	3.900	±.104	-6.650	±.145	-26.204	±.164	.105
	4	4.445	±.189	3.851	±.168	-5.994	±.213	-24.175	±.220	.143
	5	4.088	±.198	4.333	±.178	-5.034	±.222	-20.248	±.196	.091
	6	3.728	±.098	4.536	±.131	-4.357	±.105	-17.556	±.117	.081
	7	3.885	±.107	4.506	±.159	-3.788	±.122	-15.881	±.133	.051
	8	3.889	±.170	4.925	±.249	-3.447	±.193	-14.758	±.175	.084
	9	3.328	±.079	5.353	±.185	-3.085	±.080	-13.770	±.104	.068
11	11	4.312	±.504	3.609	±.274	-6.959	±.617	-25.417	±.385	.268
	12	4.500	±.175	3.550	±.150	-6.032	±.210	-21.805	±.195	.112
	13	4.281	±.113	3.581	±.142	-5.244	±.135	-18.964	±.163	.072
	14	4.411	±.110	3.883	±.159	-4.602	±.122	-16.518	±.137	.102
	15	4.348	±.095	4.251	±.161	-4.067	±.106	-15.095	±.121	.107
	16	4.359	±.119	4.128	±.180	-3.777	±.137	-13.936	±.128	.106
	17	4.162	±.088	4.199	±.147	-3.525	±.105	-12.152	±.103	.082
	24	3.805	±.357	3.287	±.360	-7.096	±.321	-28.281	±.416	.103
12	6	1.912	±.488	4.254	±.256	-8.187	±.579	-26.922	±.339	.210
	7	2.396	±.396	4.254	±.237	-7.097	±.448	-23.442	±.249	.226
	8	2.370	±.428	4.902	±.197	-5.917	±.507	-20.762	±.278	.156
	9	4.031	±.201	4.124	±.191	-6.808	±.259	-19.980	±.154	.209
	10	3.058	±.540	5.052	±.468	-4.926	±.670	-15.822	±.335	.346
	11	3.744	±.493	4.701	±.541	-5.403	±.594	-16.056	±.327	.256
	12	3.726	±.324	5.008	±.272	-4.991	±.404	-14.843	±.239	.132
	17	3.622	±.631	3.611	±.219	-9.588	±.694	-28.126	±.316	.283
	18	4.059	±.328	3.582	±.165	-8.592	±.375	-24.189	±.199	.151
	19	4.503	±.144	3.663	±.102	-7.185	±.134	-20.376	±.090	.141
	20	4.594	±.141	3.856	±.094	-6.500	±.149	-17.992	±.095	.114
	21	4.632	±.167	4.053	±.143	-5.772	±.194	-15.667	±.123	.097
	22	4.212	±.186	4.265	±.178	-5.282	±.214	-14.488	±.142	.137
	23	4.252	±.103	4.915	±.112	-4.686	±.107	-13.443	±.082	.094
	24	4.438	±.094	4.038	±.104	-3.892	±.100	-13.193	±.082	.091
	25	4.378	±.109	3.936	±.096	-4.651	±.110	-15.534	±.079	.104
	26	4.072	±.104	3.683	±.100	-5.202	±.110	-17.859	±.098	.093
	27	4.548	±.239	3.534	±.130	-6.620	±.258	-21.563	±.144	.180
	28	3.985	±.468	3.393	±.191	-7.772	±.500	-26.485	±.267	.278
16	1	4.573	±.078	3.805	±.087	-5.475	±.081	-15.842	±.084	.062
	2	3.955	±.111	3.913	±.106	-5.883	±.114	-16.838	±.092	.081
	3	4.196	±.159	3.561	±.121	-7.165	±.170	-20.882	±.149	.083
	4	4.164	±.271	3.390	±.163	-8.688	±.293	-25.164	±.241	.104
	5	4.023	±.151	3.388	±.087	-10.629	±.165	-30.696	±.158	.072
	6	3.181	±.159	3.659	±.085	-9.254	±.173	-28.111	±.137	.107
17	5	3.937	±.089	5.758	±.155	-3.569	±.094	-10.948	±.100	.086
	6	3.777	±.139	4.699	±.183	-4.075	±.144	-12.114	±.125	.142
	7	4.094	±.261	5.042	±.231	-4.721	±.292	-13.946	±.191	.115

TABLE V.- AERODYNAMIC-CENTER POSITION

Group M	Group $(X_{ac})_r$	Flight	Run	M	q_{m_R}	$(X_{ac})_{flex}$ (method I)	$(X_{ac})_{flex}$ (method II)	ΔX_{ac}	$(X_{ac})_r$ (method I)	$(X_{ac})_r$ (method II)
0.429	23.71 ± 0.52	11	24	0.427	11.4	22.1 ± 0.7	20.6 ± 0.9	3.5	25.6	24.1
		12	28	.427	11.4	21.8 ± 1.5	20.7 ± 1.4	3.5	25.3	24.2
		16	5	.428	11.5	21.3 ± 0.3	19.8 ± 0.4	3.5	24.8	23.3
		16	6	.433	11.9	20.1 ± 0.3	16.4 ± 0.5	3.6	23.7	20.0
.486	24.45 ± 0.35	12	27	.482	14.7	21.6 ± 1.2	20.8 ± 0.9	4.4	26.0	25.2
		16	4	.482	14.8	19.4 ± 0.5	18.7 ± 0.9	4.4	23.8	23.1
		12	17	.483	12.0	19.7 ± 1.2	18.0 ± 1.9	3.6	23.3	21.6
		4	21	.486	11.9	21.8 ± 0.7	21.9 ± 1.0	3.6	25.4	25.5
		11	11	.495	12.8	22.5 ± 1.6	20.3 ± 1.9	3.9	26.4	24.2
.541	24.10 ± 0.27	12	18	.532	14.8	19.7 ± 0.8	18.8 ± 1.2	4.4	24.1	23.2
		11	12	.542	15.6	21.1 ± 0.6	19.7 ± 0.7	4.6	25.7	24.3
		16	3	.542	19.0	18.1 ± 0.5	16.8 ± 0.6	5.5	23.6	22.3
		12	26	.543	19.2	19.5 ± 0.4	18.4 ± 0.4	5.5	25.0	23.9
		8	4	.544	15.5	19.9 ± 0.3	18.5 ± 0.4	4.6	24.5	23.1
.595	24.33 ± 0.31	12	6	.584	12.3	18.0 ± 1.0	14.8 ± 1.6	3.7	21.7	18.5
		4	20	.591	18.5	19.2 ± 0.4	20.6 ± 0.6	5.4	24.6	26.0
		12	25	.595	23.6	18.5 ± 0.6	18.2 ± 0.5	6.7	25.2	24.9
		11	13	.597	18.9	20.1 ± 0.3	19.2 ± 0.5	5.5	25.6	24.7
		10	3	.598	15.5	20.9 ± 0.6	19.8 ± 0.4	4.6	25.5	24.4
		9	1	.598	12.2	20.6 ± 0.4	18.8 ± 0.6	3.7	24.3	22.5
		16	2	.599	24.0	17.4 ± 0.5	15.6 ± 0.5	6.8	24.2	22.4
		12	19	.600	19.3	16.2 ± 0.5	18.3 ± 0.5	5.6	21.8	23.9
.635	24.23 ± 0.33	3	14	.631	13.9	19.2 ± 0.3	21.3 ± 0.4	4.2	23.4	25.5
		2	27	.636	13.6	21.3 ± 0.6	19.5 ± 0.4	4.1	25.4	23.6
		11	14	.637	22.1	18.7 ± 0.5	18.5 ± 0.5	6.3	25.0	24.8
		12	20	.637	22.2	16.3 ± 0.7	17.9 ± 0.6	6.3	22.6	24.2
.644	23.96 ± 0.21	12	7	.642	14.7	17.0 ± 1.1	14.9 ± 1.4	4.4	21.4	19.3
		12	24	.642	27.9	17.4 ± 0.6	16.2 ± 0.5	7.7	25.1	23.9
		16	1	.642	28.2	17.3 ± 0.4	15.8 ± 0.4	7.7	25.0	23.5
		6	15	.643	18.7	17.9 ± 0.6	17.1 ± 1.0	5.4	23.3	22.5
		9	2	.647	14.7	19.3 ± 0.3	19.7 ± 0.9	4.4	23.7	24.1
		10	4	.647	18.5	20.0 ± 0.8	19.7 ± 0.7	5.4	25.4	25.1
		8	5	.648	23.4	18.1 ± 0.3	17.0 ± 0.2	6.6	24.7	23.6
.681	24.25 ± 0.36	12	8	.679	16.6	21.1 ± 1.9	13.0 ± 1.7	4.9	26.0	17.9
		9	3	.681	16.5	19.4 ± 0.3	18.4 ± 0.3	4.9	24.3	23.3
		10	5	.681	20.5	19.9 ± 0.7	17.8 ± 0.8	5.9	25.8	23.7
		11	15	.681	25.3	19.1 ± 0.6	18.2 ± 0.5	7.1	26.2	25.3
		12	21	.682	26.2	16.5 ± 0.7	17.7 ± 0.9	7.2	23.7	24.9
.695	24.32 ± 0.28	3	13	.689	17.2	18.5 ± 0.2	18.6 ± 0.4	5.0	23.5	23.6
		6	14	.690	22.2	18.9 ± 0.8	17.7 ± 0.8	6.3	25.2	24.0
		12	22	.694	27.3	16.0 ± 0.8	15.9 ± 1.0	7.5	23.5	23.4
		4	19	.699	27.7	17.5 ± 0.3	17.9 ± 0.3	7.6	25.1	25.5
		11	16	.702	28.0	17.7 ± 0.5	17.0 ± 0.7	7.7	25.4	24.7
.726	24.44 ± 0.17	12	9	.721	19.3	17.0 ± 0.9	19.0 ± 0.9	5.6	22.6	24.6
		17	7	.725	32.2	18.0 ± 1.2	14.9 ± 1.4	8.5	26.5	23.4
		10	6	.726	25.1	17.9 ± 0.4	17.8 ± 0.4	7.0	24.9	24.8
		3	12	.728	20.6	18.5 ± 0.3	18.4 ± 0.5	5.9	24.4	24.3
		9	4	.731	20.4	18.2 ± 0.4	18.0 ± 0.8	5.9	24.1	23.9
.735	24.89 ± 0.35	11	17	.734	32.3	17.3 ± 0.5	18.1 ± 0.5	8.6	25.9	26.7
		12	23	.735	33.1	15.2 ± 0.4	15.9 ± 0.5	8.7	23.9	24.6
		2	28	.735	20.4	18.9 ± 0.6	18.4 ± 0.6	5.9	24.8	24.3
		6	13	.741	27.4	17.6 ± 0.7	16.2 ± 0.7	7.5	25.1	23.7
.758	25.53 ± 0.25	3	11	.750	22.3	17.9 ± 0.4	18.2 ± 0.7	6.4	24.3	24.6
		8	6	.758	36.3	16.8 ± 0.3	16.0 ± 0.2	9.4	26.2	25.4
		17	6	.762	38.0	15.4 ± 0.6	14.6 ± 0.7	9.7	25.1	24.3
		10	7	.763	29.6	18.8 ± 0.5	18.5 ± 0.5	8.0	26.8	26.5
.776	24.41 ± 0.14	12	10	.773	24.0	17.4 ± 2.6	17.0 ± 2.8	6.8	24.2	23.8
		9	5	.779	25.7	17.5 ± 0.2	16.9 ± 0.3	7.1	24.6	24.0
.791	26.58 ± 0.20	6	11	.789	32.2	18.4 ± 0.3	18.4 ± 0.4	8.6	27.0	27.0
		10	8	.789	31.7	18.2 ± 1.1	19.2 ± 0.9	8.5	26.7	27.7
		6	12	.790	32.8	16.7 ± 0.3	18.6 ± 0.5	8.7	25.4	27.3
		12	11	.790	26.3	18.0 ± 2.8	21.2 ± 2.6	7.3	25.3	28.5
		9	6	.795	26.7	19.7 ± 0.6	19.0 ± 0.7	7.4	27.1	26.4
		2	29	.796	26.7	19.2 ± 0.4	19.2 ± 0.4	7.4	26.6	26.6
.810	27.76 ± 0.48	17	5	.808	46.0	14.6 ± 0.4	15.7 ± 0.5	11.1	25.7	26.8
		9	7	.810	28.5	21.1 ± 0.6	22.0 ± 1.3	7.8	28.9	29.8
		10	9	.812	34.9	19.6 ± 0.4	19.7 ± 0.4	9.1	28.7	28.8
		12	12	.812	29.0	18.6 ± 1.4	21.4 ± 1.8	7.9	26.5	29.3

TABLE VI.- ZERO-LIFT WING-FUSELAGE PITCHING-MOMENT COEFFICIENTS

Group M	Group C_{m_0}	Flight	Run	M	C_{m_0} (method I)	C_{m_0} (method I corrected for zero shift)	ϵC_{m_0} (method I)	C_{m_0} (method II)	ϵC_{m_0} (method II)
0.429	-0.0371 ± 0.0023	11	24	0.427	-0.0051	-0.0285	±0.0057	-0.0402	±0.0063
		12	28	.427	-.0173	-.0313	±.0091	-.0379	±.0083
		16	5	.428	.0704	-.0319	±.0019	-.0389	±.0027
		16	6	.433	.0532	-.0358	±.0013	-.0546	±.0028
.486	-0.0365 ± 0.0012	12	27	.482	-.0266	-.0307	±.0057	-.0326	±.0033
		16	4	.482	.0501	-.0361	±.0021	-.0401	±.0046
		12	17	.483	-.0924	-.0387	±.0098	-.0448	±.0114
		4	21	.486	-.0227	-.0415	±.0035	-.0397	±.0049
		11	11	.495	.0065	-.0264	±.0069	-.0354	±.0089
.541	-0.0426 ± 0.0019	12	18	.532	-.0866	-.0388	±.0054	-.0413	±.0057
		11	12	.542	-.0081	-.0301	±.0024	-.0358	±.0030
		16	3	.542	.0383	-.0394	±.0018	-.0432	±.0025
		12	26	.543	-.0466	-.0441	±.0021	-.0452	±.0016
		8	4	.544	.1286	-.0449	±.0045	-.0515	±.0019
.595	-0.0459 ± 0.0016	12	6	.584	.1379	-.0554	±.0043	-.0823	±.0092
		4	20	.591	-.0563	-.0532	±.0027	-.0454	±.0025
		12	25	.595	-.0597	-.0452	±.0027	-.0435	±.0016
		11	13	.597	-.0212	-.0415	±.0013	-.0429	±.0018
		10	3	.598	.1851	-.0492	±.0051	-.0534	±.0025
		9	1	.598	.2981	-.0507	±.0070	-.0682	±.0034
		16	2	.599	.0242	-.0455	±.0014	-.0496	±.0029
		12	19	.600	-.0963	-.0546	±.0039	-.0379	±.0023
.635	-0.0495 ± 0.0026	3	14	.631	.0069	-.0595	±.0014	-.0465	±.0020
		2	27	.636	-.0229	-.0478	±.0033	-.0551	±.0023
		11	14	.636	-.0429	-.0446	±.0024	-.0431	±.0017
		12	20	.637	-.0954	-.0485	±.0045	-.0392	±.0022
.644	-0.0445 ± 0.0011	12	7	.642	.0914	-.0678	±.0044	-.0753	±.0074
		12	24	.642	-.0638	-.0457	±.0028	-.0448	±.0013
		16	1	.642	.0203	-.0417	±.0007	-.0445	±.0011
		6	15	.643	-.0201	-.0489	±.0033	-.0596	±.0038
		9	2	.647	.2108	-.0597	±.0102	-.0562	±.0044
		10	4	.647	.1270	-.0417	±.0038	-.0403	±.0032
		8	5	.648	.0674	-.0436	±.0014	-.0472	±.0010
.681	-0.0478 ± 0.0018	12	8	.679	.0766	-.0447	±.0073	-.0771	±.0079
		9	3	.681	.1566	-.0539	±.0053	-.0553	±.0017
		10	5	.681	.0962	-.0419	±.0025	-.0478	±.0033
		11	15	.681	-.0462	-.0441	±.0027	-.0462	±.0015
		12	21	.682	-.0942	-.0470	±.0043	-.0418	±.0025
.695	-0.0523 ± 0.0015	3	13	.689	-.0120	-.0614	±.0014	-.0585	±.0023
		6	14	.690	-.0240	-.0517	±.0040	-.0529	±.0031
		12	22	.694	-.0916	-.0505	±.0049	-.0487	±.0028
		4	19	.699	-.0615	-.0530	±.0018	-.0496	±.0009
		11	16	.702	-.0550	-.0485	±.0021	-.0483	±.0017
.726	-0.0620 ± 0.0013	12	9	.721	.0338	-.0615	±.0029	-.0514	±.0036
		17	7	.725	-.0118	-.0513	±.0037	-.0556	±.0037
		10	6	.726	.0352	-.0612	±.0009	-.0593	±.0016
		3	12	.728	-.0217	-.0651	±.0013	-.0633	±.0022
		9	4	.731	.1017	-.0728	±.0029	-.0711	±.0035
.736	-0.0586 ± 0.0016	11	17	.734	-.0632	-.0592	±.0023	-.0557	±.0013
		12	23	.735	-.0908	-.0598	±.0027	-.0547	±.0015
		2	28	.735	-.0573	-.0632	±.0039	-.0645	±.0026
		6	13	.741	-.0345	-.0654	±.0037	-.0674	±.0024
.758	-0.0637 ± 0.0007	3	11	.750	-.0275	-.0777	±.0027	-.0725	±.0028
		8	6	.758	.0168	-.0634	±.0004	-.0628	±.0005
		17	6	.762	-.0263	-.0664	±.0021	-.0653	±.0019
		10	7	.763	.0115	-.0652	±.0010	-.0629	±.0017
.776	-0.0809 ± 0.0003	12	10	.773	-.0036	-.0789	±.0088	-.0774	±.0098
		9	5	.779	.0460	-.0807	±.0015	-.0812	±.0016
.791	-0.0770 ± 0.0010	6	11	.789	-.0360	-.0733	±.0012	-.0772	±.0011
		10	8	.789	-.0065	-.0733	±.0029	-.0659	±.0028
		6	12	.790	-.0428	-.0791	±.0020	-.0772	±.0016
		12	11	.790	.0024	-.0802	±.0104	-.0673	±.0088
		9	6	.795	.0315	-.0801	±.0022	-.0798	±.0027
		2	29	.796	-.0760	-.0838	±.0036	-.0813	±.0014
.810	-0.0779 ± 0.0023	17	5	.808	-.0374	-.0760	±.0017	-.0700	±.0012
		9	7	.810	.0201	-.0866	±.0021	-.0785	±.0044
		10	9	.812	-.0102	-.0826	±.0012	-.0795	±.0013
		12	12	.812	-.0304	-.0848	±.0075	-.0715	±.0058

TABLE VII.- RADIUS-OF-GYRATION DATA

Flight	Run	$k_{y_f}^2$ (method II)	$\epsilon_{k_{y_f}^2}$ (method II)	$k_{y_f}^2$ (method I)	$\epsilon_{k_{y_f}^2}$ (method I)	$\left(k_{y_f}^2\right)_{av}$ (methods I and II)	$\left(k_{y_f}^2\right)_{calc}$	$\frac{qm_R}{W}$	$\Delta k_{y_f}^2$
2	27	370.8	±3.2	404.9	±12.9	387.8	363.0	1.208×10^{-4}	24.8
	28	357.8	±4.0	385.9	±11.5	371.8	360.7	1.834	11.1
	29	348.5	±3.7	394.1	±10.8	371.3	358.3	2.380	13.0
3	11	359.1	±4.5	371.8	±10.6	365.4	367.5	1.854	-2.1
	12	377.3	±2.5	394.7	±7.6	386.0	367.9	1.715	18.1
	13	351.6	±4.6	382.8	±9.0	367.2	369.2	1.435	-2.0
	14	404.2	±2.8	395.2	±7.3	399.7	369.9	1.168	29.8
4	19	317.0	±4.5	337.6	±5.9	327.3	335.1	2.544	-7.8
	20	341.5	±3.2	343.9	±6.9	342.7	338.3	1.702	4.4
	21	340.8	±3.8	367.5	±8.5	354.2	340.6	1.098	13.6
6	11	318.0	±2.7	365.2	±8.6	341.6	343.7	2.960	-2.1
	12	314.1	±3.0	308.9	±6.8	311.5	343.8	3.017	-32.3
	13	306.2	±3.0	331.7	±10.4	319.0	345.6	2.528	-26.6
	14	340.3	±3.9	362.4	±13.6	351.3	348.1	2.052	3.2
	15	313.5	±4.6	341.3	±11.0	327.4	349.3	1.738	-21.9
8	4	304.3	±3.4	332.3	±8.9	318.3	351.7	1.242	-33.4
	5	315.3	±1.8	337.2	±5.6	326.2	349.4	1.880	-23.2
	6	290.7	±1.5	326.3	±5.0	308.5	345.4	2.927	-36.9
9	1	344.3	±3.2	370.4	±6.2	357.3	363.9	.963	-6.6
	2	335.0	±4.7	360.4	±12.0	347.7	362.7	1.165	-15.0
	3	307.7	±3.6	360.1	±8.0	333.9	362.1	1.308	-28.2
	4	337.1	±4.9	344.3	±5.9	340.7	361.2	1.623	-20.5
	5	344.6	±2.9	333.0	±5.5	338.8	359.8	2.049	-21.0
	6	348.5	±5.8	368.5	±14.4	358.5	359.7	2.133	-1.2
	7	360.6	±9.9	362.8	±15.7	361.7	359.1	2.282	2.6
10	3	347.0	±2.0	351.8	±8.5	349.4	360.5	1.219	-11.1
	4	364.0	±3.1	380.0	±10.3	372.0	359.7	1.462	12.3
	5	334.8	±3.0	352.6	±8.1	343.7	359.3	1.623	-15.6
	6	329.6	±2.0	334.9	±4.9	332.2	357.8	1.990	-25.6
	7	332.3	±2.4	347.1	±6.4	339.7	356.9	2.360	-17.2
	8	328.2	±3.4	330.2	±11.5	329.2	356.5	2.532	-27.3
	9	327.4	±2.1	343.1	±5.8	335.2	355.8	2.794	-20.6
11	11	336.1	±4.8	361.5	±13.0	348.8	356.9	1.172	-8.1
	12	334.6	±2.8	362.7	±6.6	348.6	356.0	1.433	-7.4
	13	336.5	±2.7	358.4	±5.6	347.4	355.7	1.742	-8.3
	14	327.2	±4.3	331.5	±7.2	329.3	354.5	2.037	-25.2
	15	328.6	±2.4	343.8	±8.7	336.2	353.3	2.334	-17.1
	16	319.2	±2.6	332.4	±5.7	325.8	352.5	2.597	-26.7
	17	303.7	±2.3	309.8	±5.8	306.7	350.5	3.005	-43.8
	24	355.2	±5.0	375.4	±18.1	365.3	359.5	1.099	5.8
12	6	318.0	±3.8	334.4	±7.5	326.2	350.1	1.022	-23.9
	7	319.1	±3.2	329.7	±8.5	324.4	349.3	1.222	-24.9
	8	314.9	±2.5	336.7	±11.9	325.8	348.7	1.384	-22.9
	9	326.9	±2.3	315.9	±7.7	321.4	347.4	1.614	-26.0
	10	308.6	±6.0	302.0	±16.6	305.3	346.3	2.015	-41.0
	11	330.1	±6.1	314.0	±7.3	322.0	345.5	2.214	-23.5
	12	327.9	±4.8	309.3	±10.6	318.6	344.2	2.443	-25.6
	17	331.6	±3.6	338.7	±8.2	335.2	349.3	1.029	-14.1
	18	334.1	±2.6	337.1	±6.0	335.6	348.4	1.270	-12.8
	19	340.5	±1.4	323.3	±5.2	331.9	347.1	1.658	-15.2
	20	330.4	±1.1	317.4	±6.1	323.9	346.1	1.909	-22.2
	21	321.3	±2.3	315.1	±6.4	318.2	344.7	2.257	-26.5
	22	307.7	±2.7	308.4	±7.6	308.0	344.8	2.358	-36.8
	23	313.5	±1.7	310.5	±4.5	312.0	343.4	2.868	-31.4
	24	294.3	±1.6	311.2	±6.0	302.7	336.2	2.511	-33.5
	25	309.9	±1.5	313.2	±5.1	311.5	337.8	2.124	-26.3
	26	312.0	±1.6	330.2	±4.8	321.1	339.5	1.736	-18.4
	27	311.1	±2.0	324.2	±8.6	317.6	341.3	1.333	-23.7
	28	314.1	±3.0	333.0	±11.0	323.5	341.8	1.034	-18.3
16	1	332.9	±1.6	339.6	±4.5	336.2	354.1	2.408	-17.9
	2	324.1	±1.6	334.0	±5.8	329.0	354.3	2.055	-25.3
	3	342.9	±2.3	348.9	±7.2	345.9	354.8	1.630	-8.9
	4	347.2	±3.1	351.8	±6.4	349.5	356.7	1.276	-8.2
	5	349.8	±1.7	365.8	±5.4	357.8	358.5	.996	-.7
	6	333.3	±1.5	362.0	±3.1	347.6	358.0	1.034	-10.4
17	5	308.0	±2.4	298.3	±5.9	303.1	347.0	3.952	-43.9
	6	306.9	±2.7	315.2	±7.3	311.1	349.3	3.270	-38.2
	7	321.7	±3.9	339.3	±12.1	330.5	351.4	2.785	-20.9

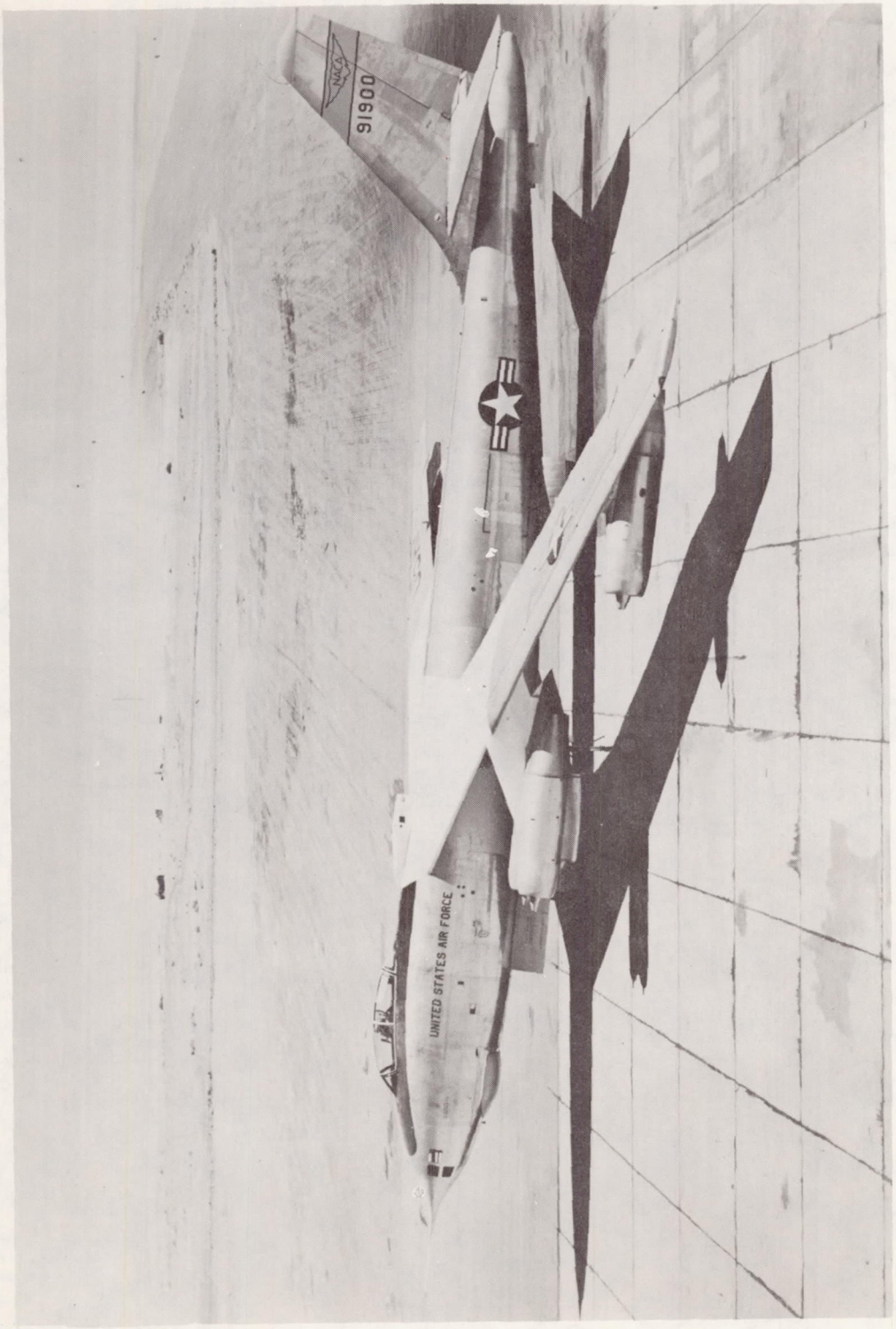

Figure 1.- Side view of test airplane. L-86692

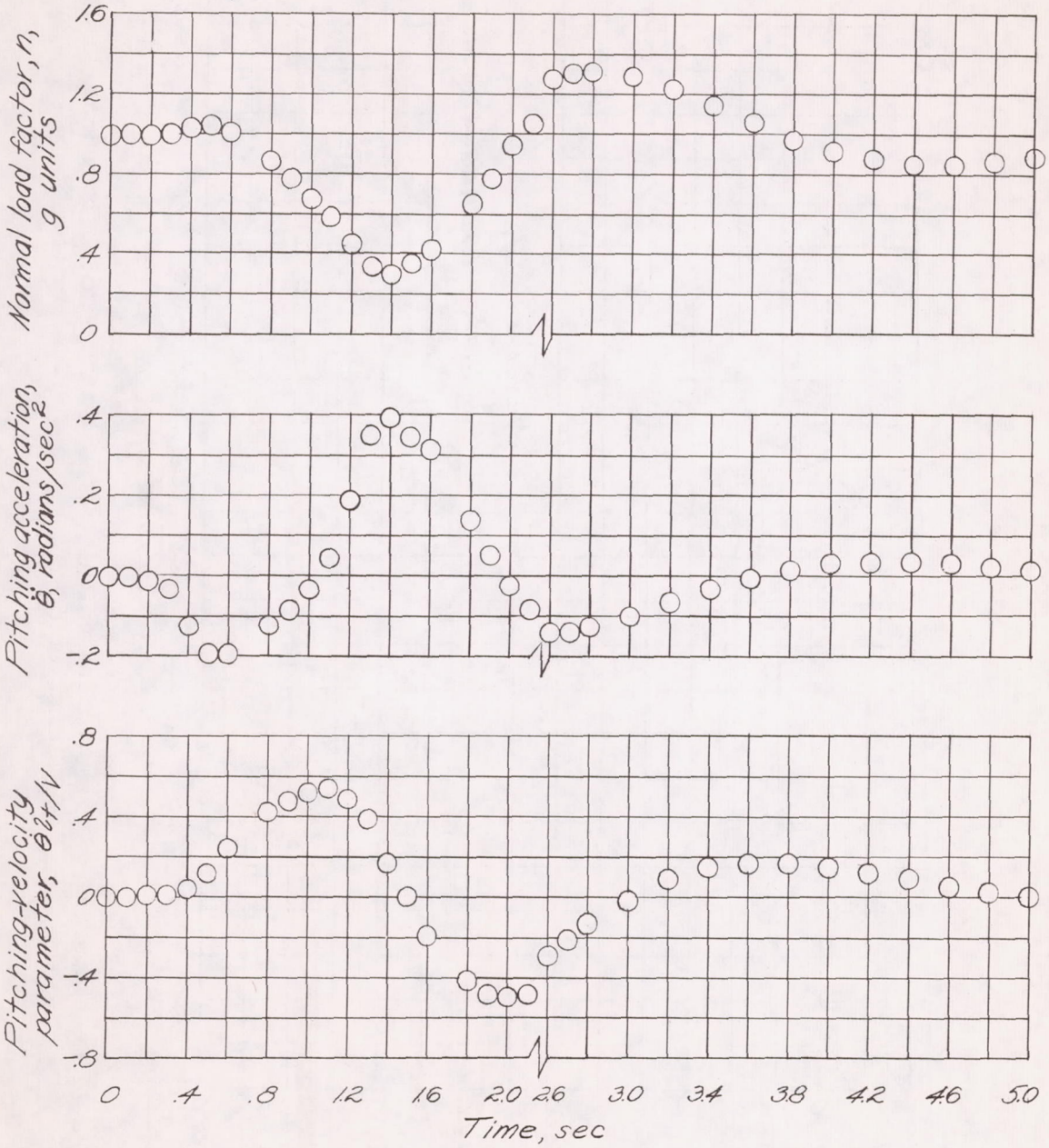

Figure 2.- Time-history data for push-pull maneuver.

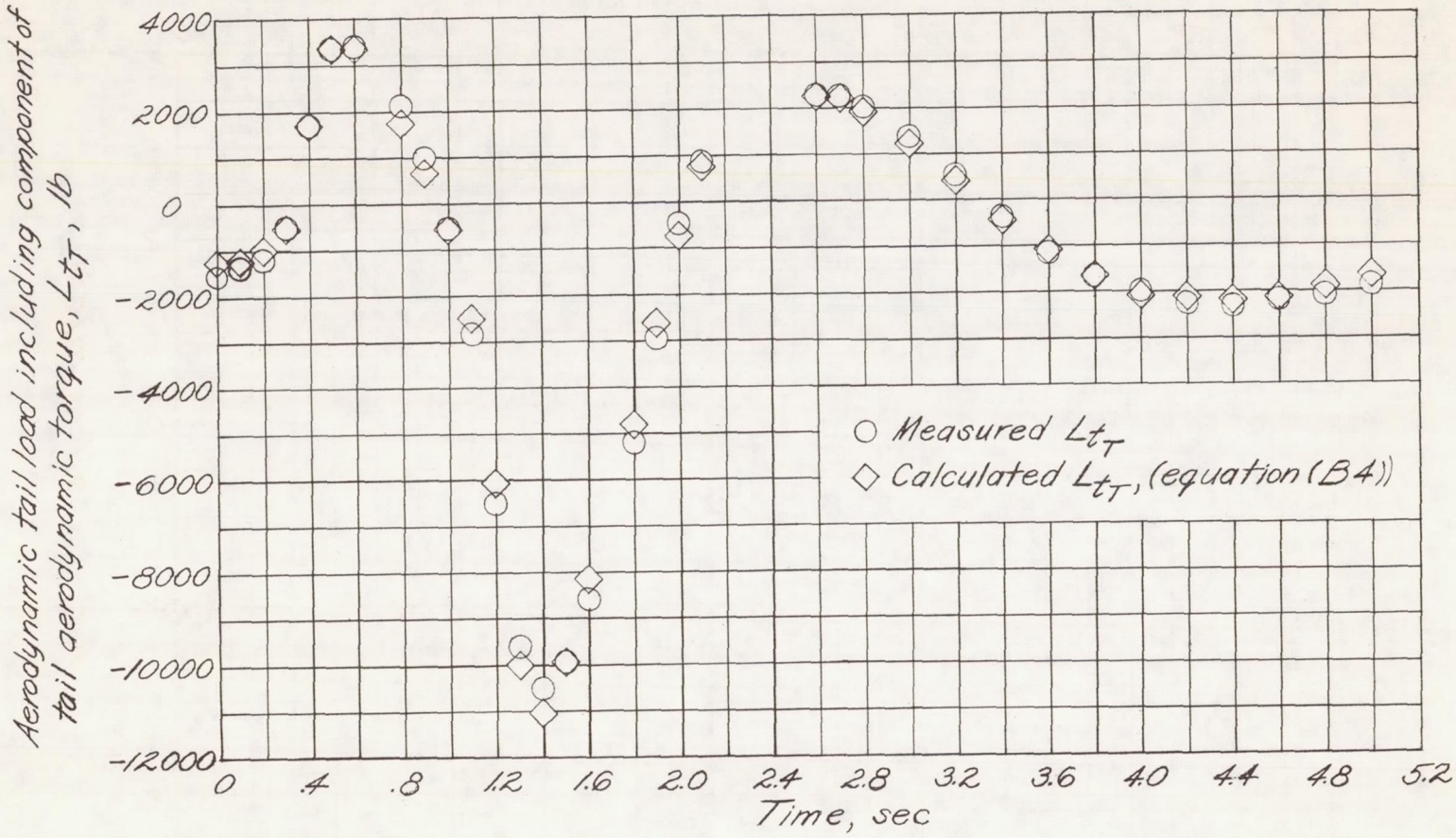

Figure 3.- Time histories of measured and calculated horizontal-tail aerodynamic loads for maneuver of figure 2.

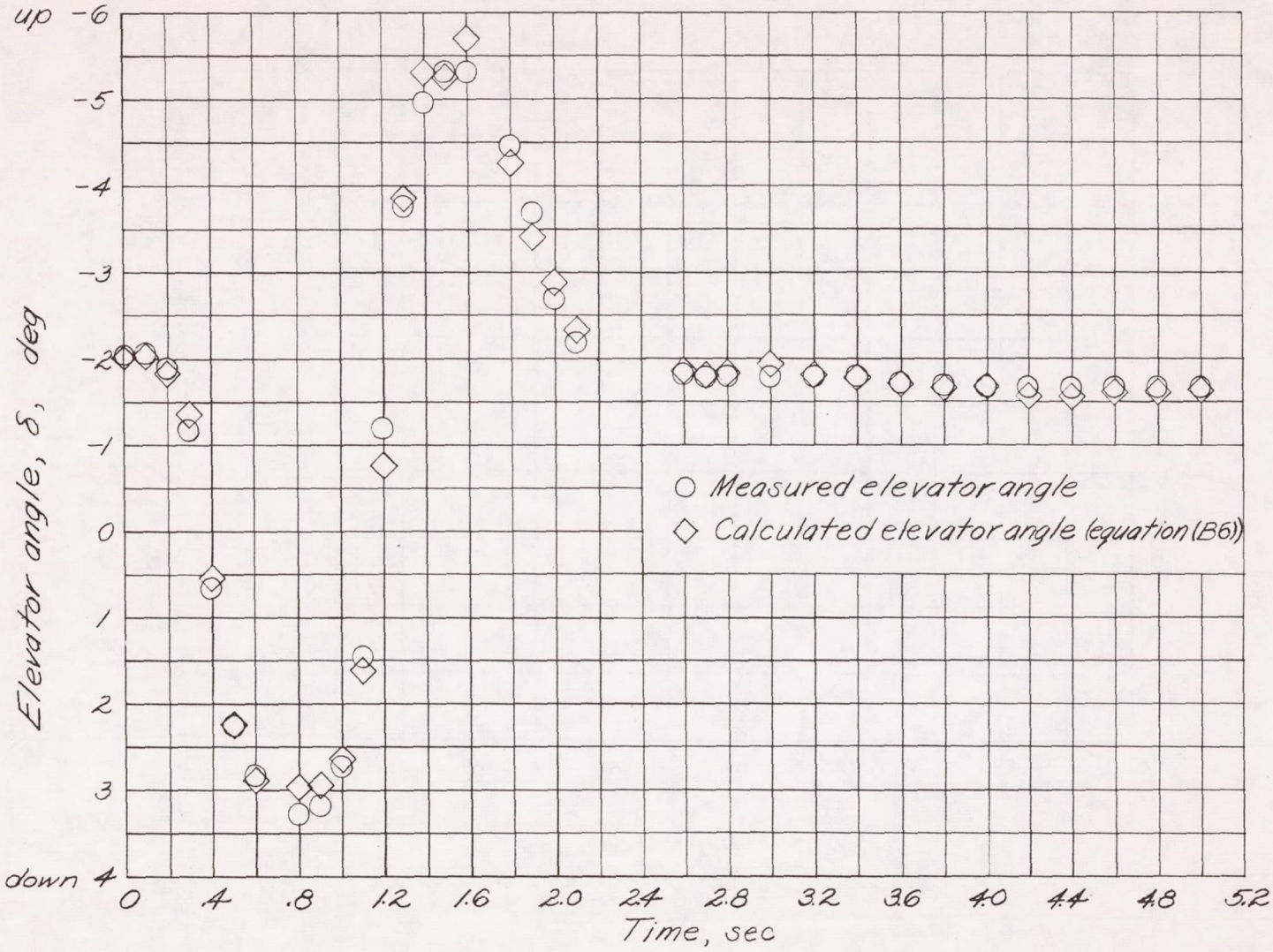

Figure 4.- Time histories of measured and calculated elevator angles for maneuver of figure 2.

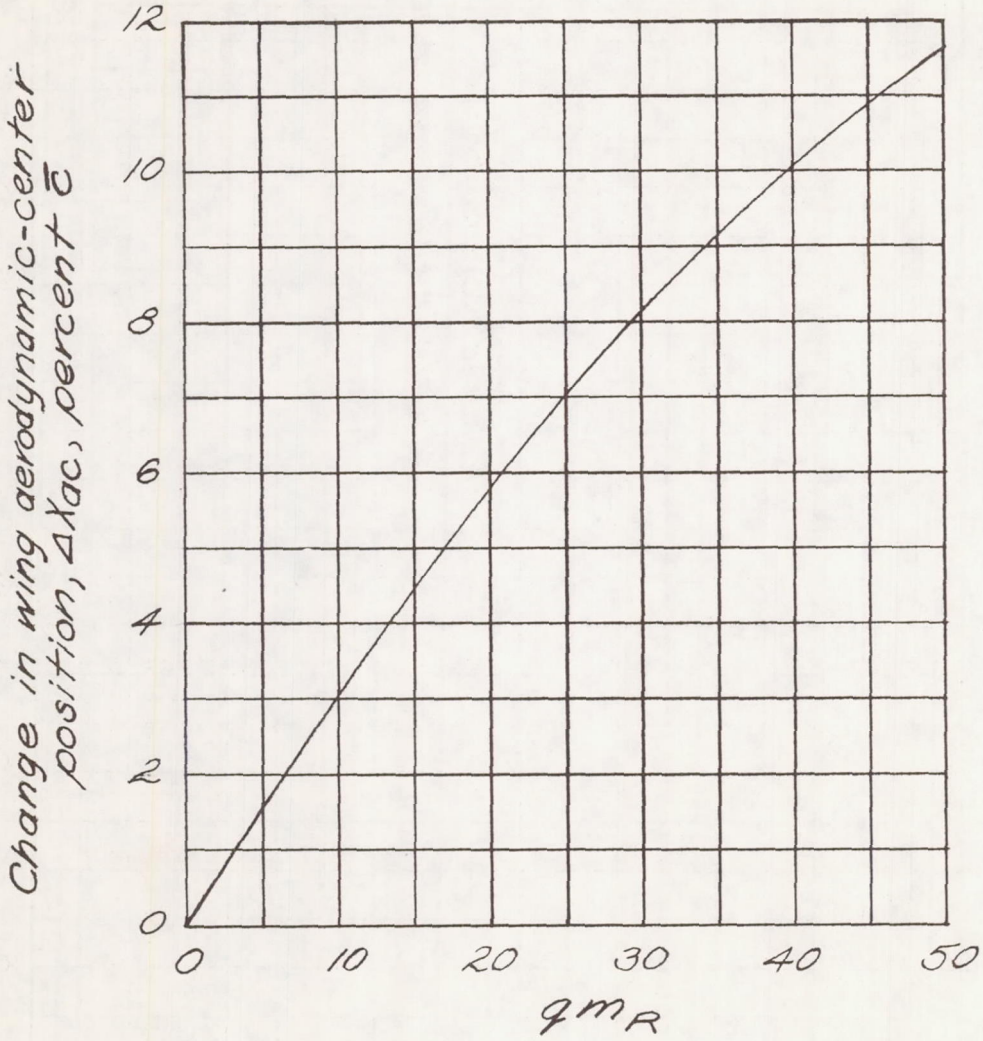

Figure 5.- Forward shift in wing aerodynamic-center position as a function of flexibility parameter from figure 4(c) of reference 5.

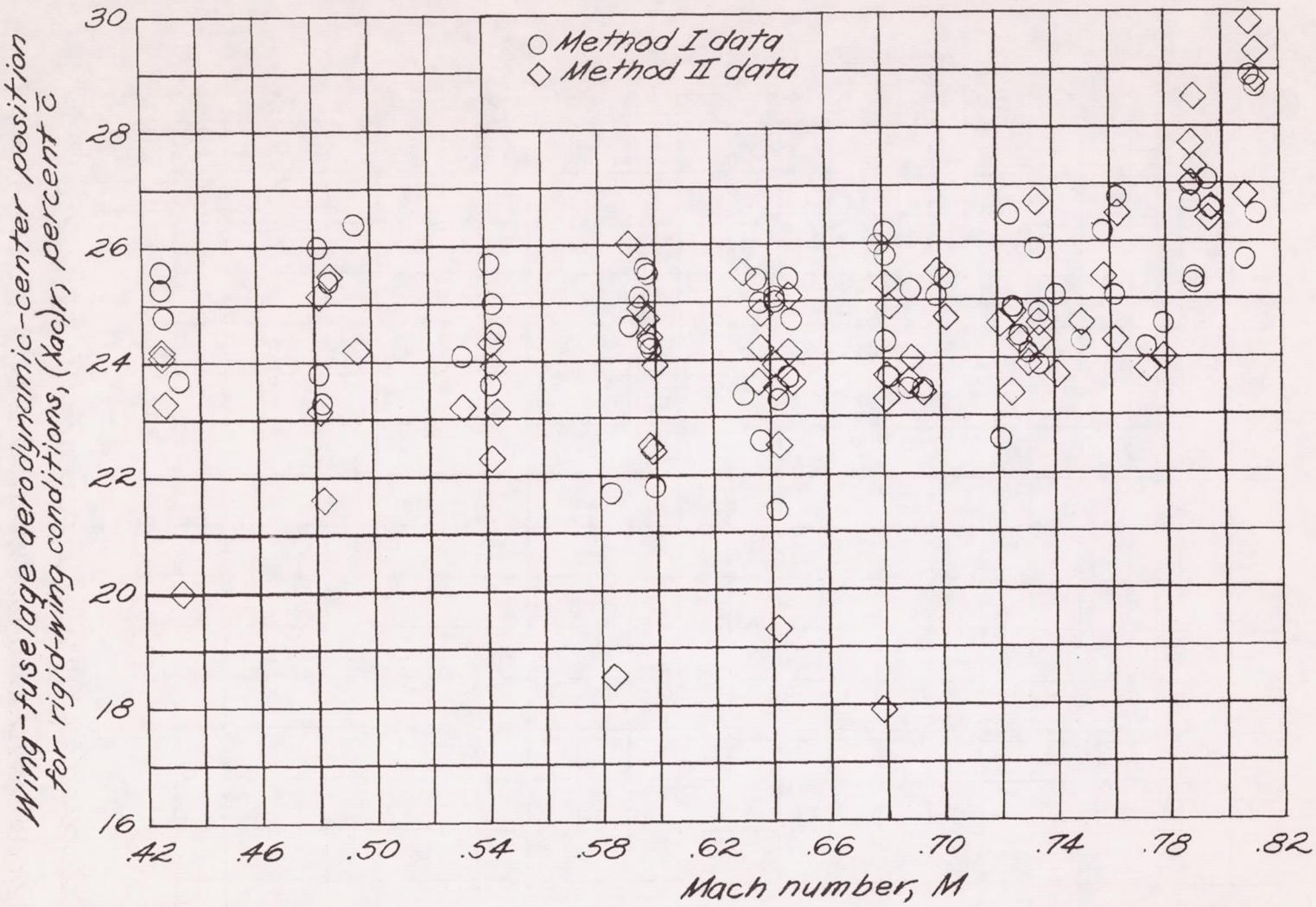

Figure 6.- Wing-fuselage aerodynamic-center data as extrapolated to rigid-wing conditions as a function of Mach number.

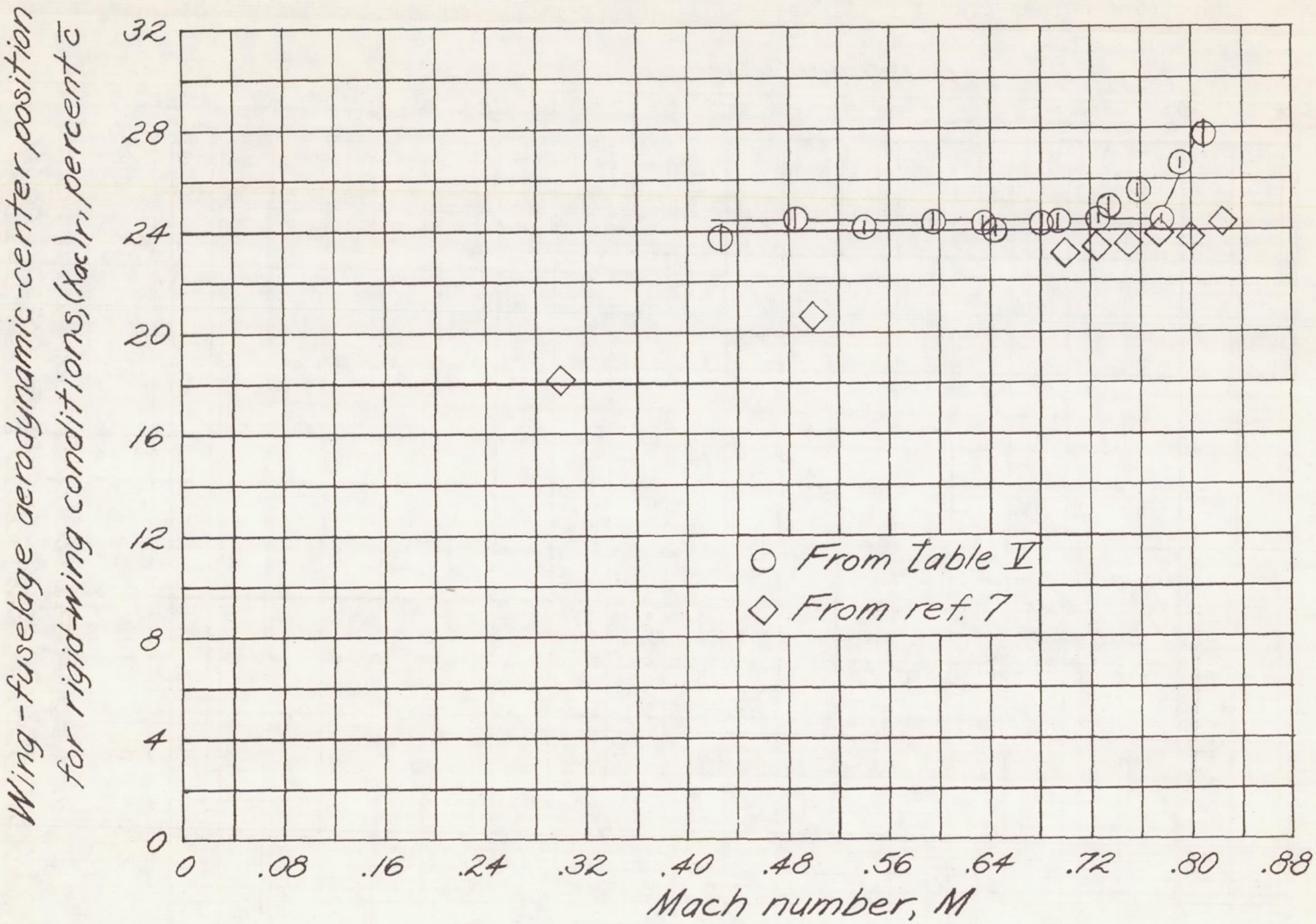

Figure 7.- Comparison of flight and wind-tunnel wing-fuselage aerodynamic-center positions for rigid-wing conditions.

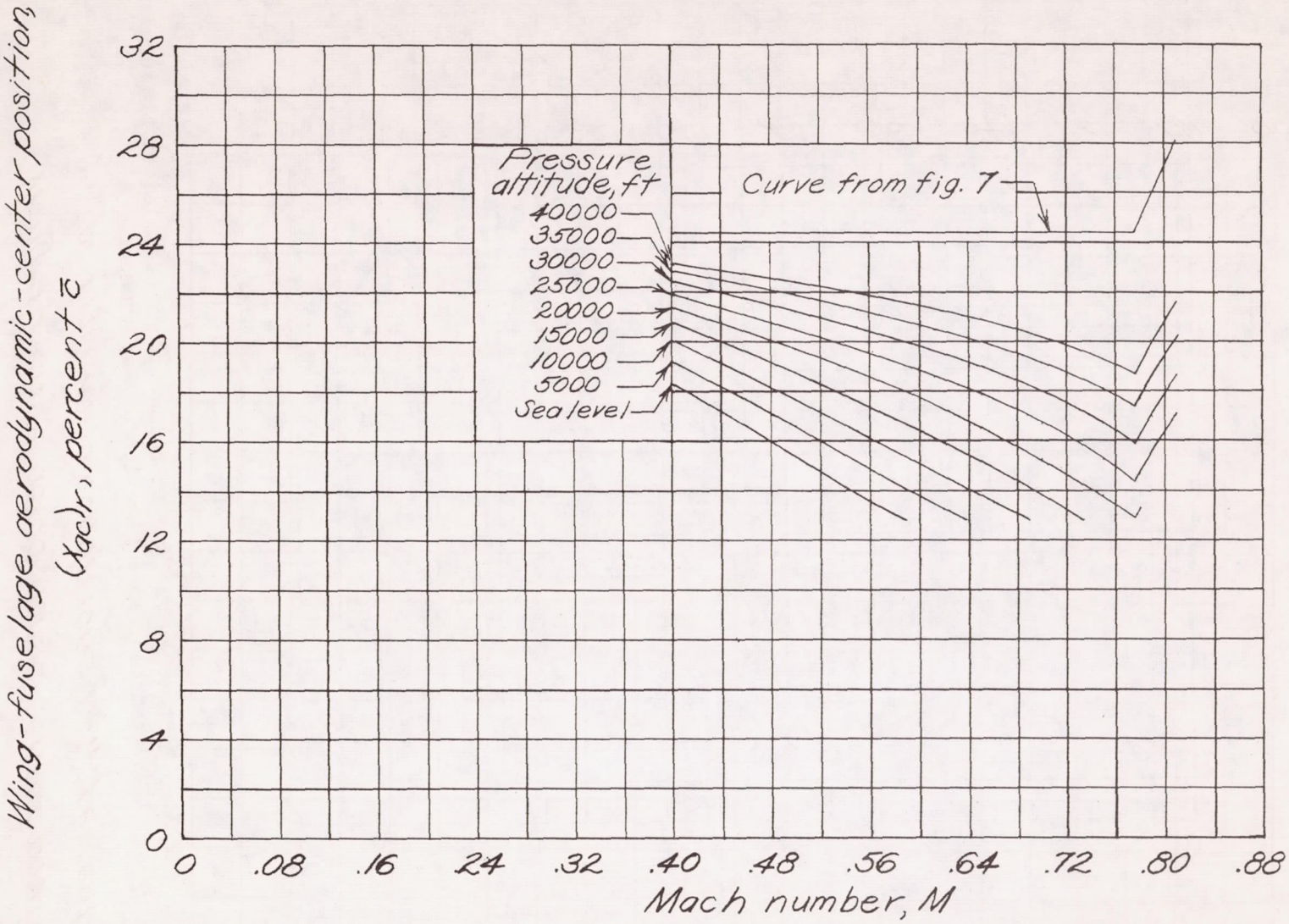

Figure 8.- Wing-fuselage aerodynamic-center position for flexible-wing conditions.

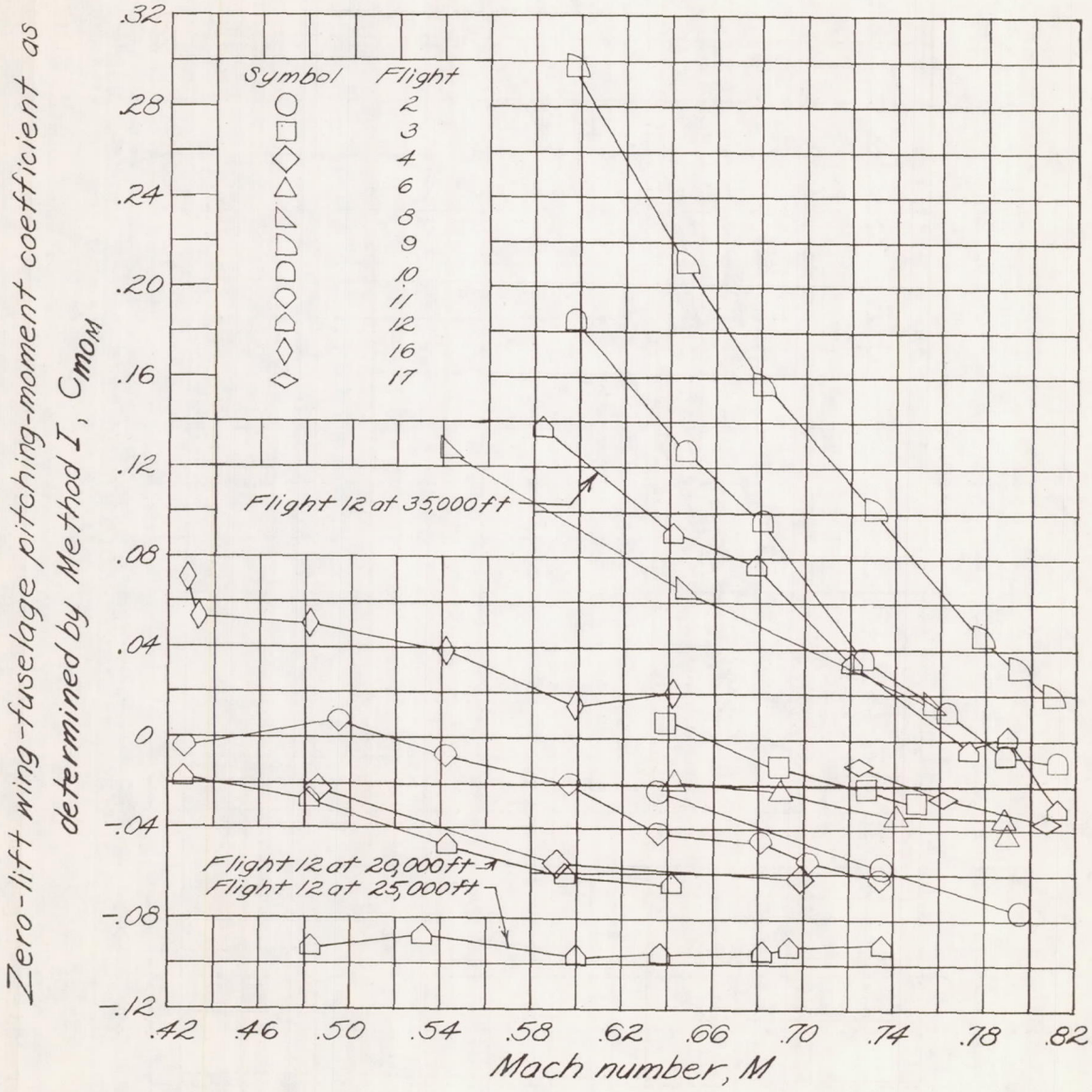

Figure 9.- Zero-lift wing-fuselage pitching-moment coefficient measured by method I as a function of Mach number.

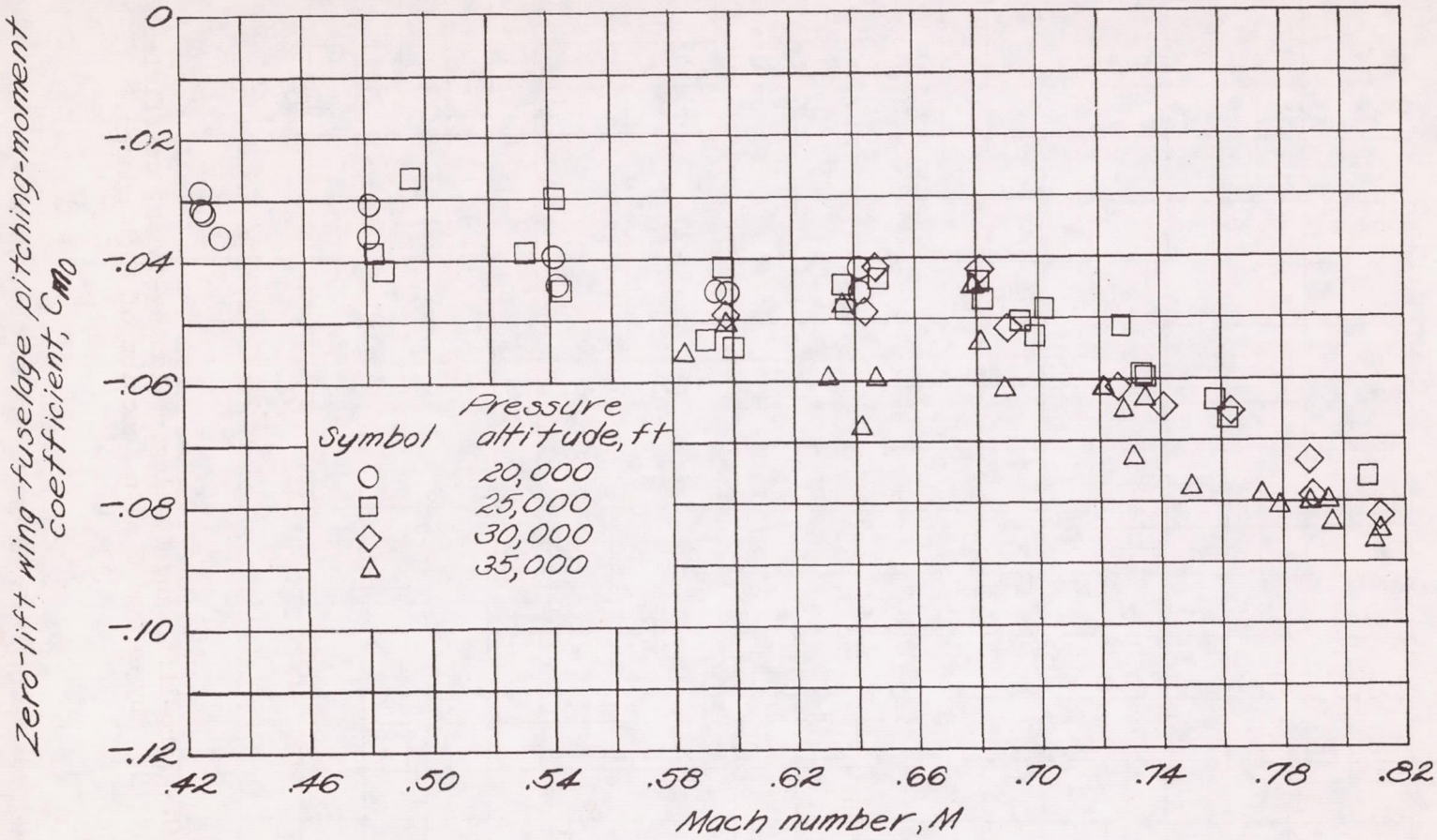

Figure 10.- Zero-lift wing-fuselage pitching-moment coefficients as obtained by method I and corrected for tail-load zero shifts.

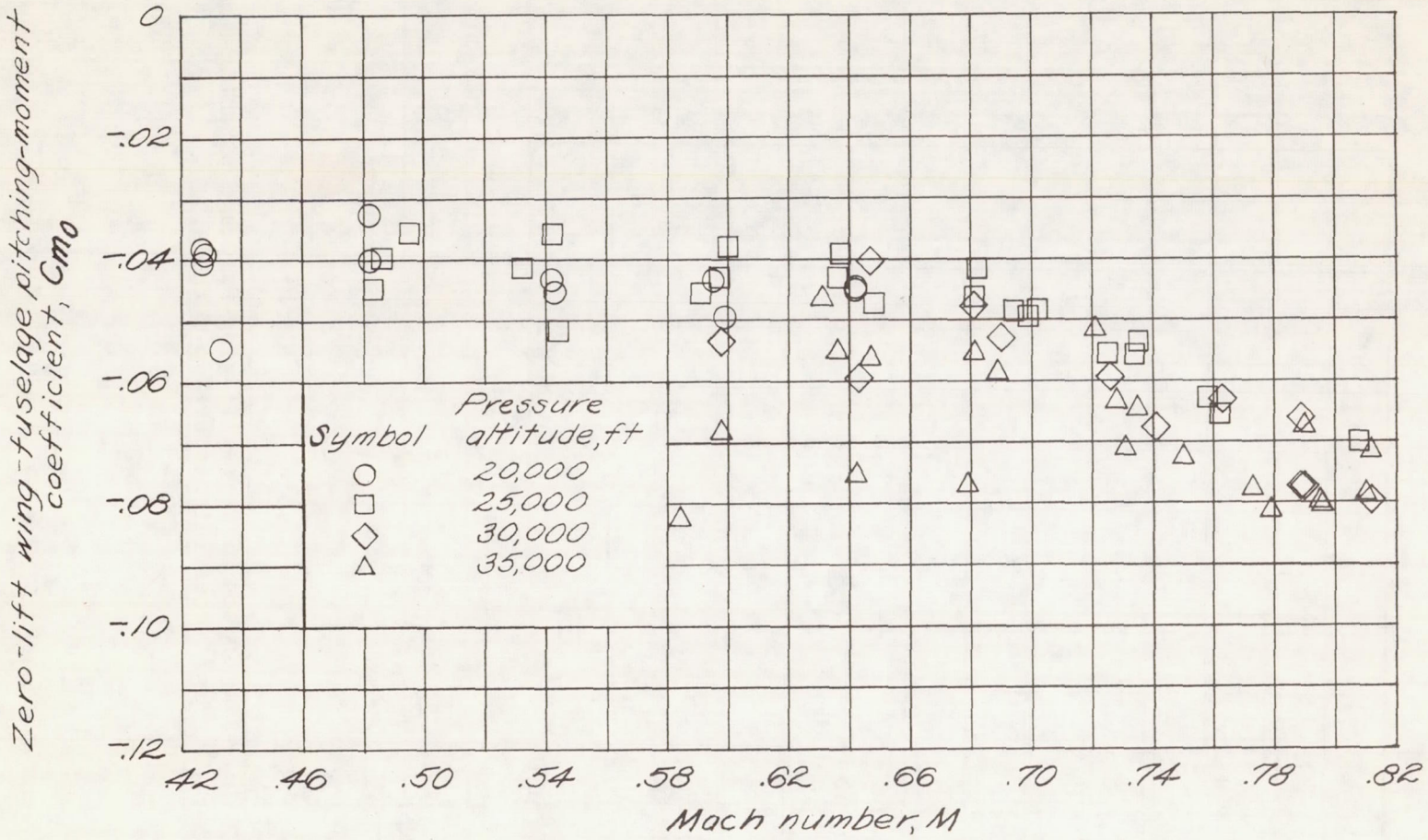

Figure 11.- Zero-lift wing-fuselage pitching-moment coefficients as obtained by method II.

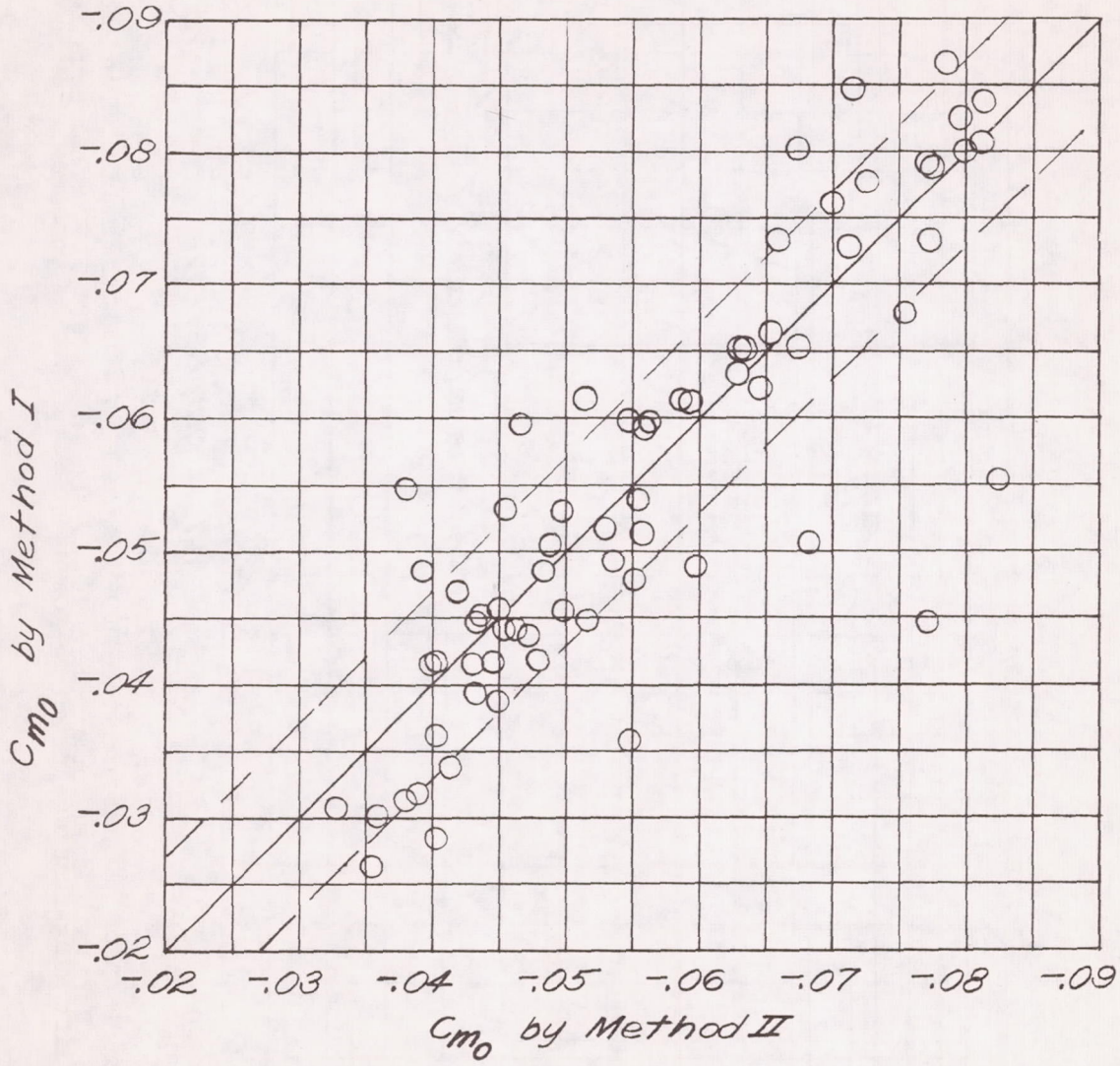

Figure 12.- Comparison of zero-lift wing-fuselage pitching-moment coefficients by two methods.

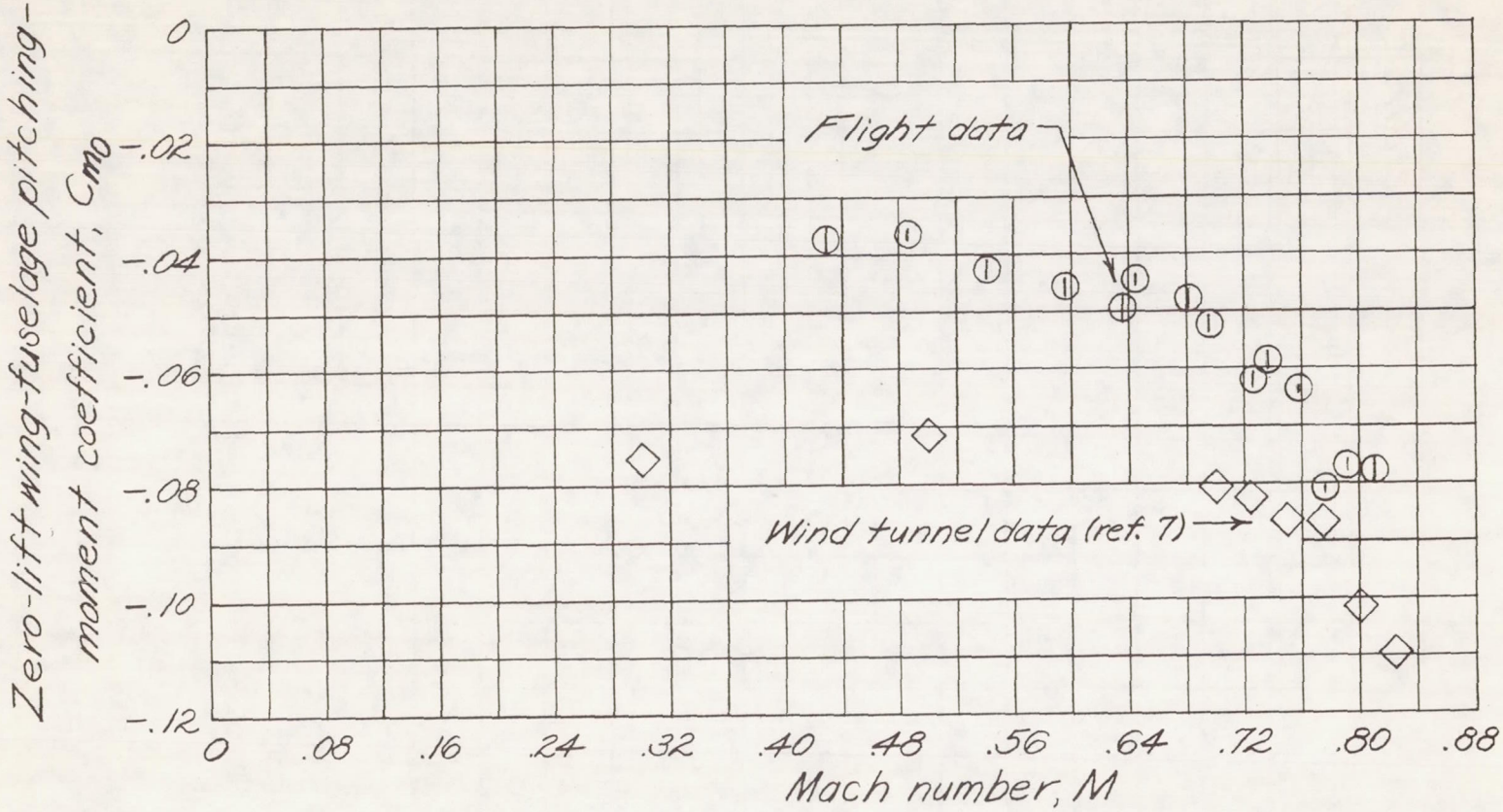

Figure 13.- Comparison of flight and wind-tunnel zero-lift wing-fuselage pitching-moment coefficients. Vertical lines in circle symbols are values of $\overline{\epsilon C_{m_0}}$ from equation (17).

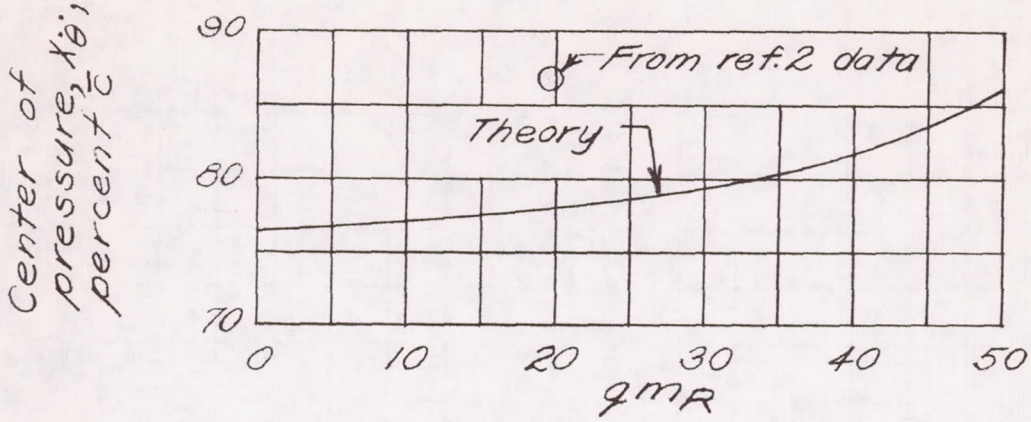

(a) Center of pressure of wing aerodynamic load due to pitching acceleration.

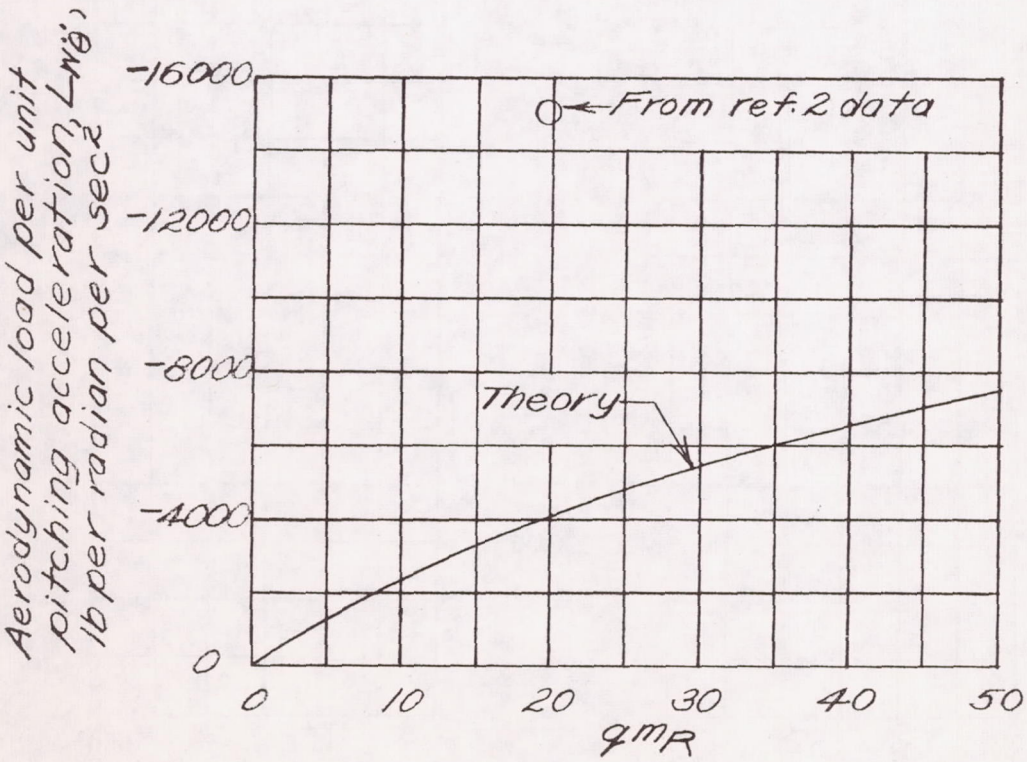

(b) Aerodynamic load due to pitching acceleration for both wings.

Figure 14.- Pitching-acceleration wing aerodynamic-load parameters as functions of flexibility parameter qm_R.

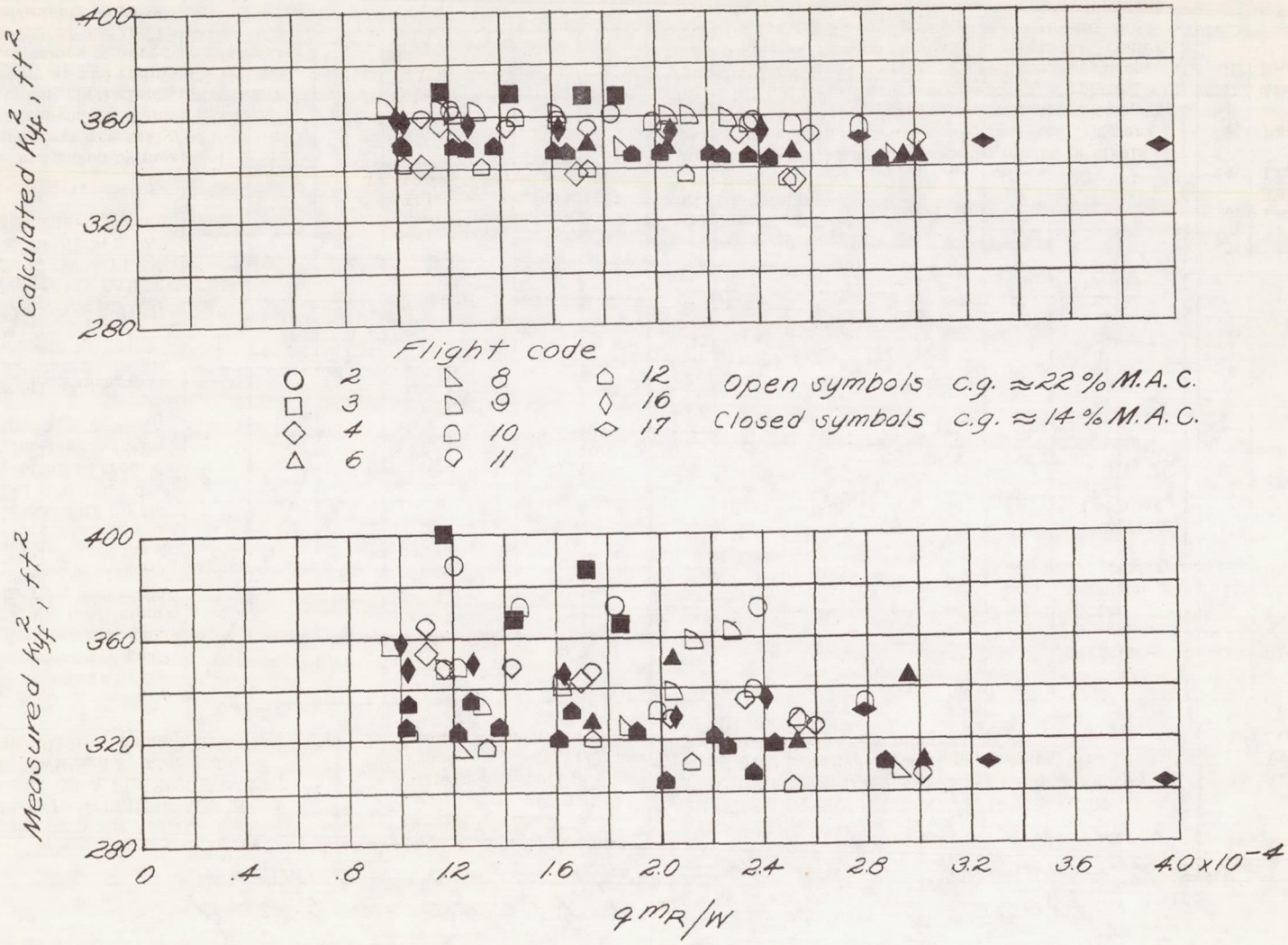

Figure 15.- Measured and calculated radii of gyration in pitch squared as function of flexibility parameter qm_R/W.